7382 *Inorg. Chem.* **2010**, *49*, 7382–7400
DOI: 10.1021/ic100666t

Inorganic Chemistry
Article

Structure, Stereochemistry, and Physico-Chemical Properties of Trinuclear and Dinuclear Metal(II) Complexes of a Phenol-Based Tetrapodal Schiff Base Ligand[⊥]

Supriya Dutta,*,[†] Papu Biswas,[†,‡] Ulrich Flörke,[§] and Kamalaksha Nag*,[†]

[†]*Department of Inorganic Chemistry, Indian Association for the Cultivation of Science, Jadavpur, Kolkata −700032, India,* [‡]*Department of Chemistry, Bengal Engineering and Science University, Shibpur, Howrah −711103, India, and* [§]*Department of Inorganic and Analytical Chemistry, Paderborn University, D-33098, Paderborn, Germany*

Received April 8, 2010

The tetrapodal ligand 1,1,1,1-tetrakis[(salicylaldimino)methyl]methane (H_4L) has been used to synthesize a number of divalent metal complexes, which include (i) the trinuclear compounds $[Mg_3(HL)_2]\cdot nH_2O$ (**1**), $[Ni_3(HL)_2]\cdot 2C_7H_8$ (**3**), $[Ni_3L'_2]\cdot 0.5C_7H_8$ (**4**), $[Co_3(HL)_2]$ (**5**), and $[Co_3L'_2]\cdot C_6H_6$ (**6**); (ii) the dinuclear compounds $[Ni_2L]$ (**2**), $[Cu_2L]\cdot CH_3CN$ (**8**), and $[Pd_2L]$ (**9**); (iii) an unusual dimeric compound $[\{Ni(H_{2.5}L)\}_2](ClO_4)\cdot 2H_2O$ (**7**); and (iv) the inclusion compounds $[Ni_2L{\subset}NaClO_4]\cdot CH_3CN$ (**10**) and $[Cu_2L{\subset}NaClO_4]$ (**11**). The molecular structures of compounds **1**, **3**, **4**, **6**, **7**, and **10** have been determined. In $[M_3(HL)_2]$ complexes, one of the salicylaldimine chelating units remains uncoordinated, which on being hydrolyzed is transformed to the amine-ending complex $[M_3L'_2]$. All of the trinuclear complexes have the same core coordination sphere $[N_3M(\mu\text{-}O_{phenolate})_3M(\mu\text{-}O_{phenolate})_3MN_3]$ where the terminal metals are connected to the central metal via face-shared phenolate oxygens. In the trinuclear compounds, the terminal metals are distorted from octahedral to trigonal prismatic to different extents in **1** and **6**, while in **3** and **4** they are trigonal antiprismatically distorted. The stereochemical configurations obtained by the terminal metals in **3** and **6** are homochiral ($\Delta\cdots\Delta$), but heterochiral ($\Lambda\cdots\Delta$) in **1** and **4**. In compound **7**, the two mononuclear complex units are held together by three equivalent $O\cdots H\cdots O$ bridges, indicating 50% deprotonation of all the metal-coordinated phenols. The temperature-dependent magnetic behavior of **7** has indicated the presence of very weak antiferromagnetic exchange coupling ($J = -0.2\ cm^{-1}$) between the two nickel(II) centers. Very similar magnetic behavior observed for the trinuclear nickel(II) compounds **3** and **4** is attributed to a ferromagnetic exchange interaction between the adjacent metals ($J = 7.6\ cm^{-1}$), although an interaction between the terminal metals is absent; in contrast, the adjacent cobalt(II) centers in **6**, however, are involved in an antiferromagnetic exchange interaction ($J = -5.7\ cm^{-1}$). The dinuclear complexes $[M_2L]$, in which each of the metal centers are chelated with a pair of salicylaldimines, act as hosts (when M = Ni and Cu) for alkali metals (Li^+, Na^+, and K^+). The host−guest binding constants (K) have been determined in $(CH_3)_2SO$ solution, and the results show that $[Ni_2L]$ is a better host compared to $[Cu_2L]$. The decreasing order of K values for both hosts is $Na^+ > Li^+ > K^+$. $[Ni_2L{\subset}NaClO_4]\cdot CH_3CN$ (**10**) has been shown to have a polymeric structure in which sodium is octahedrally surrounded by four nickel-coordinated phenolate and two perchlorate oxygens. The magnesium(II) complex **1** exhibits strong fluorescence in CH_2Cl_2 at room temperature with $\lambda_{em} = 425$ nm, and the lifetime for fluorescent decay is 18.5 ns. The thermal behaviors of **3** and **6** with regard to their loss of aromatic solvent molecules have been studied. The evolution of the toluene molecules from **3** takes place between 140° and 230 °C, while the benzene is evolved between 100° and 180 °C in **6**. The enthalpy of desolvation of **3** is 43.4 kJ mol^{-1}.

Introduction

Polypodal ligands are metal binding scaffolds that produce metal complexes with interesting structures, properties, and reactivities.[1−3] Indeed, they have turned out to be much sought after ligands for designing structural and functional models of many metalloenzymes.[4−7] When these ligands

---

[⊥] This work is dedicated to Professor Animesh Chakravorty, IACS, on the occasion of his 75th birthday.

*Author to whom correspondence should be addressed. Fax: +91-33-2473-2805. E-mail: ickn@iacs.res.in.

(1) For recent reviews, see: (a) Chomitz, W. A.; Arnold, J. *Chem.*—*Eur. J.* **2009**, *15*, 2020. (b) Blackman, A. J. *Eur. J. Inorg. Chem.* **2008**, 2633. (c) Dai, Z.; Canary, J. W. *New J. Chem.* **2007**, *31*, 1708. (d) Blackman, A. G. *Polyhedron* **2005**, *24*, 1. (e) Hu, X.; Meyer, K. *J. Organomet. Chem.* **2005**, *690*, 5474.

(2) (a) Trofimenko, S. *Scorpionates: Polypyrazolylborate Ligands and Their Coordination Chemistry*; World Scientific Publishing Company: Singapore, 1999. (b) Trofimenko, S. *Chem. Rev.* **1993**, *93*, 943. (c) Dias, H. V. R.; Lovely, C. J. *Chem. Rev.* **2008**, *108*, 3223.

(3) Grohmann, A. *Adv. Inorg. Chem.* **2004**, *56*, 179.

(4) Kitajima, N.; Moro-oka, Y. *Chem. Rev.* **1994**, *94*, 737.

(5) Gavrilova, A. L.; Bosnich, B. *Chem. Rev.* **2004**, *104*, 349.

(6) (a) Vahrenkamp, H. *Dalton Trans.* **2007**, 4751. (b) Weston, J. *Chem. Rev.* **2005**, *105*, 2151. (c) Perkin, G. *Chem. Rev.* **2004**, *104*, 987.

Chart 1

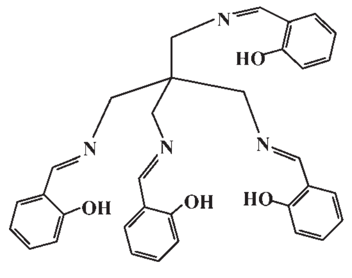

H_4L

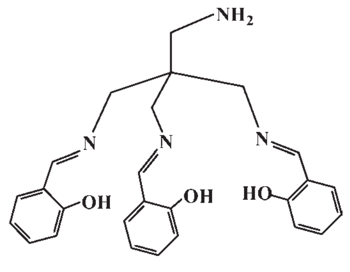

H_3L'

contain proton dissociating chelating moieties, they form complexes with high thermodynamic stabilities,[8] which find applications as diagnostic and therapeutic agents. For instance, robust gadolinium(III) chelates derived from several tetrapodal ligands are widely used as MRI contrast agents.[9] Again, metal sequestering polypodal chelating agents are used as antidotes for metal intoxication,[10] especially for removing plutonium(IV) and other actinides from body system.[11]

The tripodal ligand 1,1,1-tris[(salicylideneamino)methyl]-methane (H_3tsmm) was first introduced by Dwyer et al.[12] as a potential hexadentate chelating agent for iron(III). Since then, a number of studies have been reported for complexes of several other trivalent metals[13−16] as well as complexes of tetravalent manganese,[16] technitium,[17] and silicon,[18] obtained with related Schiff base ligands, especially 1,1,1-tris-[(salicylideneamino)methyl]ethane (H_3tsme). In recent years, Kojima and co-workers have reported[19] that, aside from mononuclear complexes, H_3tsme is capable of forming homo- and heterometallic di- and trinuclear complexes, including the 3d−4f combinations $M^{II}Ln^{III}$ and $M^{II}Ln^{III}M^{II}$. Over the past few years, Chandrasekhar et al.[20] have opened up several interesting aspects of the chemistry of homo- and heterotrinuclear $M^{II}M^{II}M^{II}$, $M^{II}M'^{II}M^{II}$, and $M^{II}Ln^{III}M^{II}$ complexes derived from the phosphorus-anchored salicylhydrazone ligands $S{=}P[CH_3N{-}N{=}CH{-}C_6H_3{-}2{-}OH{-}3{-}H/OCH_3]_3$. The groups of Kojima and Chandrasekhar have been particularly interested in the magnetic properties of the 3d−4f systems[19b,c,f,g,20c−20g] because of their potentiality to act as single molecule magnets. It is of interest to note that both H_3tsme and the hydrazone derivatives have in common three pendant salicylaldimine units for metal binding, although their bridge heads are different.

For quite some time, we have been exploring various aspects of the chemistry of metal chelates that can be obtained from the functionalized derivatives of the tetrapodal amine 1,1,1,1-tetrakis(2-aminomethyl)methane.[21] Herein, we report the synthesis, structure, stereochemistry, reactivity, and Na^+-ion binding as well as spectroscopic, magnetic, and thermal behavior of dinuclear and trinuclear metal(II) complexes of several divalent metal ions that are obtained with the tetrapodal Schiff base ligand 1,1,1,1-tetrakis[(2-salicylaldimino)methyl]methane H_4L and its hydrolyzed derivative H_3L' (shown in Chart 1).

Experimental Details

Materials. Reagent grade chemicals obtained from commercial sources were used as received. Solvents were purified and dried according to standard methods.[22] Acetylacetonates of copper(II), cobalt(II), and nickel(II) were prepared according to the reported methods.[23] The tetrapodal amine hydrochloride

---

[7] (a) Kryatov, S. V.; Rybak-Akimova, E. V.; Schindler, S. *Chem. Rev.* **2005**, *105*, 2175. (b) Costas, M.; Mehn, M. P.; Jensen, M. P.; Que, L., Jr. *Chem. Rev.* **2004**, *104*, 939. (c) Tshuva, E. Y.; Lippard, S. J. *Chem. Rev.* **2004**, *104*, 987. (d) Kim, E.; Chufan, E.; Kamraj, K.; Karlin, K. D. *Chem. Rev.* **2004**, *104*, 1077. (e) Mirica, L. M.; Ottenwaelder, X.; Stack, T. D. P. *Chem. Rev.* **2004**, *104*, 1013. (f) Lewis, E. A.; Tolman, W. B. *Chem. Rev.* **2004**, *104*, 1047. (g) Wu, A. J.; Penner-Hahn, J. E.; Pecoraro, V. L. *Chem. Rev.* **2004**, *104*, 903.

[8] (a) Raymond, K. N.; Dertz, E. A.; Kim, S. S. *Proc. Natl. Acad. Sci. U. S.A.* **2003**, *100*, 3584. (b) Abergel, R. J.; Warner, J. A.; Shuh, D. K.; Raymond, K. N. *J. Am. Chem. Soc.* **2006**, *128*, 8920 and the references therein.

[9] (a) Caravan, P.; Ellison, J. E.; McMurray, T. J.; Lauffer, R. L. *Chem. Rev.* **1999**, *99*, 2293. (b) Marbach, A. E.; Toth, E. *The Chemistry of Contrast Agents in Medical Magnetic Resonance Imaging*; John Wiley & Sons: New York, 2001.

[10] Anderssen, O. *Chem. Rev.* **1999**, *99*, 2683.

[11] Gorden, A. E.; Xu, J.; Raymond, K. N.; Durbin, P. *Chem. Rev.* **2003**, *103*, 4207.

[12] Dwyer, F. P.; Gill, N. S.; Gyarfas, E. C.; Lions, F. *J. Am. Chem. Soc.* **1957**, *79*, 1269.

[13] Green, M. A.; Welch, M. J.; Huffman, J. C. *J. Am. Chem. Soc.* **1984**, *106*, 3689.

[14] Evans, D. F.; Jakubovic, D. A. *J. Chem. Soc., Dalton Trans.* **1988**, 2927.

[15] Liu, S.; Wong, E.; Karunaratne, V.; Rettig, S. J.; Orvig, C. *Inorg. Chem.* **1993**, *32*, 1756.

[16] Drew, M. G. B.; Harding, C. J.; McKee, V.; Morgan, G. G.; Nelson, J. *J. Chem. Soc., Chem. Commun.* **1995**, 1035.

[17] Marimon, M. E.; Woulfe, S. R.; Newmann, W. L.; Pilcher, G.; Nosco, D. N. *Nucl. Med. Med. Biol.* **1996**, *23*, 567.

[18] Kojima, M.; Azuma, S.; Hirotsu, M.; Nakajima, K.; Nonoyama, M.; Yoshikawa, Y. *Chem. Lett.* **2000**, 482.

[19] (a) Ohta, H.; Harada, K.; Irie, K.; Kashino, S.; Kambe, T.; Sakane, G.; Shibahara, T.; Takamizawa, S.; Mori, W.; Nonoyama, M.; Hirotsu, M.; Kojima, M. *Chem. Lett.* **2001**, 842. (b) Yamaguchi, T.; Sunatsuki, Y.; Kojima, M.; Akashi, H.; Tsuchimoto, M.; Re, N.; Osa, S.; Matsumoto, N. *Chem. Commun.* **2004**, 1048. (c) Kobayashi, T.; Yamaguchi, T.; Ohta, H.; Sunatsuki, Y.; Kojima, M.; Re, N.; Nonoyama, M.; Matsumoto, N. *Chem. Commun.* **2006**, 1950. (d) Yamaguchi, T.; Sunatsuki, Y.; Ishida, H. *Acta Crystallogr., Sect. C* **2008**, *64*, m156. (e) Sunatsuki, Y.; Kobayashi, T.; Harada, K.; Yamaguchi, T.; Nonoyama, M.; Kojima, M. *Bull. Chem. Soc. Jpn.* **2008**, *81*, 716. (f) Yamaguchi, T.; Sunatsuki, Y.; Ishida, H.; Kojima, M.; Akashi, H.; Re, N.; Matsumoto, N.; Pochaba, A.; Mrozinski, J. *Bull. Chem. Soc. Jpn.* **2008**, *81*, 598. (g) Yamaguchi, T.; Sunatsuki, Y.; Ishida, H.; Kojima, M.; Akashi, H.; Re, N.; Matsumoto, N.; Pochaba, A.; Mrozinski, J. *Inorg. Chem.* **2008**, *47*, 5736.

[20] (a) Chandrasekhar, V.; Azhakar, R.; Andavan, G. T. S.; Krishnan, V.; Zacchini, S.; Bickley, J. F.; Steiner, A.; Butcher, R. J.; Kögerler, P. *Inorg. Chem.* **2003**, *42*, 5989. (b) Chandrasekhar, V.; Azhakar, R.; Zacchini, S.; Bickley, J. F.; Steiner, A. *Inorg. Chem.* **2005**, *44*, 4608. (c) Chandrasekhar, V.; Pandian, B. M.; Azhakar, R.; Vittal, J. J.; Cle'rac, R. *Inorg. Chem.* **2007**, *46*, 5140. (d) Chandrasekhar, V.; Pandian, B. M.; Boomishankar, R.; Steiner, A.; Cle'rac, R. *Dalton Trans.* **2008**, 5143. (e) Chandrasekhar, V.; Pandian, B. M.; Boomishankar, R.; Steiner, A.; Vittal, J. J.; Houri, A.; Cle'rac, R. *Inorg. Chem.* **2008**, *47*, 4918. (f) Chandrasekhar, V.; Azhakar, R.; Pandian, B. M.; Bickley, J. F.; Steiner, A. *Eur. J. Inorg. Chem.* **2008**, 1116. (g) Chandrasekhar, V.; Pandian, B. M.; Vittal, J. J.; Cle'rac, R. *Inorg. Chem.* **2009**, *48*, 1148.

[21] Dutta, S. Transition Metal Complexes of Polypodal Ligands, Ph. D. Thesis, Jadavpur University, Kolkata, India, 2009.

[22] Perrin, D. D.; Armarego, W. L.; Perrin, D. R. *Purification of Laboratory Chemicals*, 2nd ed.; Pergamon: Oxford, U.K. 1980.

[23] (a) Fernelius, W. C.; Bryant, B. E. *Inorg. Synth.* **1957**, *5*, 105. (b) Ellern, J. B.; Ragsdale, R. O. *Inorg. Synth.* **1968**, *11*, 83.

$C(CH_2NH_2)_4 \cdot 4HCl$ was prepared by modifying[21] a procedure reported in the literature.[24]

Physical Measurements. Elemental (C, H, and N) analyses were performed on a Perkin-Elmer 2400 II elemental analyzer. IR spectra were recorded using KBr disks on a Shimadzu FT-IR 8400S spectrophotometer. The electronic absorption spectra were recorded using a Perkin-Elmer 950 UV–vis–NIR spectrophotometer, while the emission spectra were recorded on a Perkin-Elmer LS55 luminescence spectrophotometer. Lifetime measurements for the decay of photoexcited states were carried out with a Horiba Jobin YVON Fluoromax–P steady state spectrometer. For time-correlated single photon counting (TCSPC) measurements, a picosecond diode laser (IBH Nanoled-07) in an IBH Fluorocube apparatus was used. Positive-ion electrospray ionization mass spectra (ESI-MS) were obtained on a Micromass Qtof YA 264 mass spectrometer. ^1H NMR spectra were recorded on a Bruker Avance DPX spectrometer at 300 MHz or a Bruker Avance III 500 MHz NMR spectrometer with chemical shifts (δ, ppm) relative to tetramethylsilane (TMS). Room temperature (298 K) magnetic moment measurements were carried out using a Sherwood Scientific magnetic balance. Variable-temperature (2–300 K) magnetic susceptibility measurements were carried out on an MPMS Quantum Design SQUID magnetometer. The magnetic field applied was 1.0 T. Diamagnetic corrections were made by using Pascal's constant. Thermogravimetric analysis (TGA) and differential thermal analysis (DTA) were performed on an SDT Q600 thermal analyzer under flowing nitrogen, with a heating rate of 5 °C min^{-1}. Around 5 mg of the sample was used for analysis. Differential scanning calorimetric (DSC) measurements were carried out on a Perkin-Elmer Diamond DSC instrument under an argon atmosphere with the same heating rate as used for TGA/DTA. Electrochemical measurements were carried out in dimethyl sulfoxide (DMSO) at 25 °C under a nitrogen atmosphere using a Bioanalytical Systems BAS 100B electrochemical analyzer. The concentration of the supporting electrolyte tetramethylammonium perchlorate (TEAP) was 0.1 M, while that of the complex was 1 mM. Cyclic voltammetric (CV) and square wave voltammetric (SWV) measurements were carried out with a three-electrode assembly comprising either a glassy carbon or platinum working electrode, a platinum auxiliary electrode, and an aqueous Ag/AgCl reference electrode. Under the given experimental conditions, the potential of the external standard ferrocene/ferrocenium (Fc/Fc^+) couple was measured at +0.425 V vs Ag/AgCl.

Ligand Synthesis. 1,1,1,1-Tetrakis[(2-salicylaldimino)methyl]-methane (H_4L). To a suspension of $C(CH_2NH_2)_4 \cdot 4HCl$ (2.78 g, 10 mmol) in methanol (150 mL) was added triethylamine (4.04 g, 40 mmol), and the mixture was stirred at room temperature. To the resulting clear solution was added slowly a methanol solution (50 mL) of salicylaldehyde (4.89 g, 40.0 mmol), and stirring was continued for 3 h. The golden yellow solution was concentrated on a rotary evaporator when the product got deposited. This was filtered and recrystallized from a dichloromethane–hexane mixture. Yield: 4.66 g (85%). Mp: 140 °C. Anal. Calcd for $C_{33}H_{32}N_4O_4$: C, 72.26: H, 5.84; N, 10.21. Found: C, 72.20; H, 5.80; N, 10.15. FT-IR (KBr, υ/cm^{-1}): 3051 (w), 2920 (w), 2891 (w), 2844 (w), 1631 (s), 1581 (m), 1495 (s), 1460 (m), 1439 (m), 1415 (m), 1375 (m), 1344 (w), 1280 (s), 1213 (m), 1149 (m), 1114 (w), 1070 (w), 1045 (m), 1026 (m), 980 (w), 821 (m), 760 (s), 684 (w), 658 (w). ^1H NMR (300 MHz, $CDCl_3$): δ 13.22 (s, 4H, PhO*H*); 8.43 (s, 4H, C*H*=N); 7.34 (t, 4H, J_1 = 8.54 Hz, J_2 = 8.53 Hz, Ar); 7.25 (d, 4H, J = 9.05 Hz, Ar); 6.98 (d, 4H, J = 8.23 Hz, Ar); 6.90 (t, 4H, J_1 = 7.53 Hz, J_2 = 7.28 Hz, Ar); 3.78 (s, 8H, CH_2). UV (λ_{max}/nm ($\varepsilon/M^{-1}cm^{-1}$)) in CH_2Cl_2: 258 (50 000), 320 (17 300).

Preparation of Metal Complexes. ***Caution!*** *Perchlorate salts used in this study are potentially explosive and therefore should be handled in small quantities with care.*

$[Mg_3(HL)_2] \cdot nH_2O$ (1). To a solution of H_4L (0.55 g, 1 mmol) in acetonitrile (25 mL) was added successively 0.30 g (2.99 mmol) of acetylacetone mixed with methanol (5 mL) and a piece of metallic magnesium (41 mg, 1.7 mmol). The solution was stirred and heated to boiling for 0.5 h, after which 0.3 g (3 mmol) of triethylamine in 5 mL of acetonitrile was added. Heating and stirring were continued for 1 h, during which time a yellow crystalline product deposited. This was collected by filtration and recrystallized from a dichloromethane–acetonitrile mixture (yield: 0.56 g (90%)). The same product can also be obtained, albeit in reduced yield (45%), by reacting H_4L (2 equiv) with $Mg(ClO_4)_2 \cdot 6H_2O$ (3 equiv) and triethylamine (6 equiv) in acetonitrile. Because of an indefinite number of water molecules in **1**, it was fully dehydrated by heating at 100 °C for elemental analysis. Anal. Calcd for $C_{66}H_{58}N_8O_8Mg_3$: C, 68.15; H, 4.99; N, 9.63. Found: C, 68.21; H, 4.94; N, 9.56. ESI-MS (positive) in CH_2Cl_2: *m*/*z* 1164.16 $[Mg_3(HL)_2H]^+$ (100%). FT-IR (KBr, υ/cm^{-1}): 3431 (m, br), 3049 (w), 3026 (w), 2893 (m), 2665 (w), 1622 (s), 1601 (s), 1545 (s), 1477 (s), 1450 (s), 1402 (s), 1371 (w), 1344 (s), 1325 (s), 1278 (m), 1221 (m), 1198 (m), 1155 (m), 1128 (w), 1012 (m), 900 (m), 852 (w), 798 (m), 758 (s), 740 (m), 596 (m), 543 (m), 435 (m). ^1H NMR (500 MHz, CD_2Cl_2): δ 12.79 (s, 2H, ArO*H*); 8.46 (s, 2H, C*H*=N); 8.12 (s, 6H, C*H*=N (Mg)); 7.29 (t, 4H, J_1 = 8.32, J_2 = 8.12 Hz, Ar); 6.92 (d, 4H, J = 7.39, Ar); 6.90–6.87 (m, 4H, Ar); 6.54 (d, 6H, J = 8.13 Hz, Ar); 6.41 (t, 6H, J_1 = 7.45 Hz, J_2 = 7.70 Hz, Ar); 6.15 (t, 6H, J_1 = 7.88, J_2 = 7.64 Hz, Ar); 3.74 (s, 12H, CH_2 (Mg)); 3.61 (s, 4H, CH_2). UV (λ_{max}/nm ($\varepsilon/M^{-1}cm^{-1}$)) in CH_2Cl_2: 262 (10 200), 348 (53 000).

$[Ni_2L]$ (2). A mixture of $Ni(acac)_2 \cdot 4H_2O$ (0.33 g, 1.0 mmol), H_4L (0.275 g, 0.50 mmol), and triethylamine (0.20 g, 2 mmol) in acetonitrile (50 mL) was heated under reflux for 1 h, and compound **2** was deposited as brown microcrystals in near quantitative yield (0.31 g, 95%). Compound **2**. Anal. Calcd for $C_{33}H_{28}N_4O_4Ni_2$: C, 59.87; H, 4.23; N, 8.47. Found: C, 60.06; H, 4.20; N, 8.56. FT-IR (KBr, υ/cm^{-1}): 3047 (w), 2920 (w), 2860 (w), 1622 (s), 1539 (s), 1454 (s), 1352 (w), 1330 (w), 1269 (w), 1224 (w), 1203 (w), 1140 (m), 908 (w), 733 (m), 617 (w). ^1H NMR (500 MHz, $(CD_3)_2NDCO$): δ 8.36 (s, 4H, C*H*=N); 7.91 (t, 4H, Ar); 7.37 (d, 4H, Ar); 6.52 (m, 8H, Ar); 3.56 (s, 8H, CH_2). ^1H NMR (500 MHz, $(CD_3)_2SO$): δ 108, 40, 12.41, 7.66, 6.58, 5.87. UV–vis–NIR (λ_{max}/nm ($\varepsilon/M^{-1}cm^{-1}$)) in $(CH_3)_2NHCO$: 315 (11 500), 355 (11 300), 425 (10 800), 595 (80); in $(CH_3)_2SO$: 310 (9600), 365 (11 800), 415 (9000), 590 sh (120), 860 (10), 1250 (4). μ_{eff} (298 K) = 0.23 μ_B.

$[Ni_3(HL)_2] \cdot 2C_7H_8$ (3) and $[Ni_3(L')_2] \cdot 0.5C_7H_8$ (4). The reaction involving $Ni(acac)_2 \cdot 4H_2O$ (0.49 g, 1.49 mmol), H_4L (0.55 g, 1 mmol), and triethylamine (0.30 g, 3 mmol) in acetonitrile (70 mL) was carried out in the same way as described for **2**. A brown product that precipitated from the boiling solution was found to be **2** and was removed by filtration. The filtrate was evaporated to dryness, and the residue was extracted with hot benzene. After partial removal of benzene, an equal volume of toluene was added, and the solution was allowed to evaporate slowly at 60 °C. At the sign of incipient crystallization, the source of heating was removed, and the solution was kept undisturbed. Compounds **3** and **4**, which crystallized out simultaneously as dark brown rectangles and light chocolate needles, respectively, were collected by filtration, and the two compounds were separated by hand-picking under a microscope. Yield: 0.15 g (**3**) (27%) and 0.045 g (**4**) (10%).

Compound **3**. Anal. Calcd for $C_{80}H_{74}N_8O_8Ni_3$: C, 66.20; H, 5.10; N, 7.72. Found: C, 66.23; H, 5.08; N, 7.87. ESI-MS (positive) in CH_2Cl_2: *m*/*z* 1267.74 $[Ni_3(HL)_2H]^+$ (100%). FT-IR (KBr, υ/cm^{-1}): 2904 (w), 2849 (w), 1630 (s), 1599 (s), 1541 (s), 1470 (s), 1446 (s), 1400 (m), 1342 (w), 1313 (m), 1277 (w), 1215 (w), 1196 (m), 1153 (m), 1030 (w), 1016 (w), 899 (w), 754 (m), 737 (m), 592 (w), 468 (w). ^1H NMR (500 MHz, CD_2Cl_2): δ 140; 48.8;

---

[24] Fleischer, E. B.; Gebala, A. E.; Levey, A.; Tasker, P. A. *J. Org. Chem.* **1971**, *36*, 3042.

30.7; 25.2; 11.87; 7.62; 7.41; 7.36; 7.24, 7.19, 7.05, 6.78, 3.63, 2.36, −0.95. UV−vis−NIR (λ_{max}/nm (ε/M^{-1}cm^{-1})) in CH_2Cl_2: 320 (11 200), 370 (22 000), 545 (25), 930 (30).

Compound **4**. Anal. Calcd for $C_{55.5}H_{54}N_8O_6Ni_3$: C, 60.26; H, 4.88; N, 10.13. Found: C, 60.34; H, 4.98; N, 10.20. ESI-MS (positive) in CH_2Cl_2: *m*/*z* 1059.75 $[Ni_3(L')_2H]^+$ (45%); 530.42 $[Ni_3(L')_22H]^{2+}$ (100%). FT-IR (KBr, *υ*/cm^{-1}): 3280 (w), 3018 (w), 2891 (w), 1628 (s), 1599 (s), 1541 (s), 1470 (s), 1444 (s), 1398 (m), 1340 (w), 1313 (s), 1196 (m), 1153 (m), 1130 (w), 1031 (w), 1007 (w), 889 (w), 754 (m), 740 (m), 592 (m), 472 (w). ^{1}H NMR (500 MHz, CD_2Cl_2): δ 141, 48.6, 30.7, 25.3, 7.35, 3.60, 2.35, −1.05. UV−vis−NIR (λ_{max}/nm (ε/M^{-1}cm^{-1})) in CH_2Cl_2: 325 (9800), 380 (18 000), 555 (30), 950 (20).

$[Co^{II}_3(HL)_2]$ (5) and $[Co^{II}_3(L')_2]\cdot C_6H_6$ (6). The cobalt(II) complexes were prepared under a nitrogen atmosphere using standard Schlenk techniques. To a degassed acetonitrile solution (100 mL) of $Co(acac)_2\cdot 2H_2O$ (0.27 g, 0.92 mmol) were added H_4L (0.33 g, 0.60 mmol) and triethylamine (0.18 g, 1.78 mmol), and the solution was heated under reflux for 2 h. The light pink solution turned to mauve, and eventually an orange product (**5**) that was deposited was collected by filtration. The filtrate was evaporated to dryness, and the residue was extracted with hot benzene, which on slow evaporation afforded red crystals of **6**.

Compound **5**. Yield: 0.25 g (65%). Anal. Calcd for $C_{66}H_{58}N_8O_8Co_3$: C, 62.51; H, 4.57; N, 8.84. Found: C, 62.80; H, 4.62; N, 9.09. ESI-MS (positive) in CH_3CN: *m*/*z* 634.13 $[Co_3(HL)_2\text{-}2H]^{2+}$ (100%), 1268.25 $[Co_3(HL)_2H]^+$ (25%). FT-IR (KBr, *υ*/cm^{-1}): 2910 (w), 1628 (s), 1599 (w), 1543 (m), 1470 (m), 1446 (m), 1400 (w), 1342 (w), 1319 (m), 1278 (w), 1196 (m), 1151 (w), 900 (w), 758 (m). UV−vis−NIR (λ_{max}/nm (ε/M^{-1}cm^{-1})) in DMF: 365 (26 000), 580 sh, 1020 (26).

Compound **6**. Yield: 85 mg (25%). Anal. Calcd for $C_{58}H_{54}N_8O_6Co_3$: C, 61.27; H, 4.75; N, 9.86. Found: C, 61.21; H, 4.80; N, 9.84. ESI-MS (positive) in CH_3CN: *m*/*z* 1059.06 $[Co_3(L')_2H]^+$ (100%), 529.03 $[Co_3(L')_22H]^{2+}$ (70%). FT-IR (KBr, *υ*/cm^{-1}): 3430 (br, w), 2910 (w), 1628 (s), 1599 (w), 1543 (m), 1470 (m), 1446 (m), 1400 (w), 1342 (w), 1319 (m), 1278 (w), 1196 (m), 1151 (w), 900 (w), 758 (m). ^{1}H NMR (500 MHz, CD_2Cl_2): δ 231, 104.6, 7.38, −0.35, −17.46, −33.32.

$[\{Ni(H_{2.5}L)\}_2](ClO_4)\cdot 2H_2O$ (7). An acetonitrile solution (60 mL) of H_4L (0.55 g, 1.0 mmol) and $Ni(ClO_4)_2\cdot 6H_2O$ (0.37 g, 1.01 mmol) was treated with 0.15 g (1.48 mmol) of triethylamine. The solution was kept at room temperature for slow evaporation, and **7** deposited as a green crystalline product (0.42 g, 70%). X-ray diffraction quality crystals were obtained by diffusing hexane to a dichloromethane solution of **7**. Anal. Calcd for $C_{66}H_{65}N_8O_{14}Ni_2Cl$: C, 58.79; H, 4.82; N, 8.31. Found: C, 58.70; H, 5.08; N, 8.22. ESI-MS (positive) in MeCN: *m*/*z* 1210.46 $[\{Ni(H_{2.5}L)\}_2]^+$ (100%). FT-IR (KBr, *υ*/cm^{-1}): 3437 (w, br), 3060 (w), 3040 (w), 2918 (w), 2858 (w), 1635 (s), 1604 (m), 1448 (m), 1404 (w), 1280 (m), 1217 (w), 1120 (m), 1091 (m), 900 (w), 750 (s), 623 (w), 463 (w). μ_{eff} (298 K) = 3.1 μ_B. UV−vis−NIR (λ_{max}/nm (ε/M^{-1}cm^{-1})) in DMF: 320 (24 300), 360 (15 600), 420 (9000), 580 (40), 950 (60).

$[Cu_2(L)]\cdot CH_3CN$ (8) and $[Pd_2L]$ (9). These two compounds were prepared in the same way as described for **2** by reacting together $M(acac)_2$ (M = Cu, Pd), H_4L, and triethylamine in a 2:1:4 ratio in boiling acetonitrile.

Compound **8**. Yield: 70%. Anal. Calcd for $C_{35}H_{31}N_5O_4Cu_2$: C, 58.98; H, 4.35; N, 9.83. Found: C, 59.07; H, 4.27; N, 9.97. ESI-MS (positive) in MeCN: *m*/*z* 671.39 $[Cu_2(L)H]^+$ (100%). FT-IR (KBr, *υ*/cm^{-1}): 3049 (w), 2902 (w), 2856 (w), 1626 (s), 1537 (s), 1468 (m), 1450 (s), 1394 (w), 1348 (w), 1325 (m), 1278 (w), 1196 (m), 1144 (m), 1126 (w), 908 (w), 744 (w), 729 (m), 603 (w). μ_{eff} (298 K) = 3.2 μ_B.

Compound **9**. Yield: 90%. Anal. Calcd for $C_{33}H_{28}N_4O_4Pd_2$: C, 52.31; H, 3.69; N, 7.39. Found: C, 52.40; H, 3.80; N, 7.42. FT-IR (KBr, *υ*/cm^{-1}): 3433 (m, br), 3055 (w), 2930 (w), 1606 (s), 1537 (s), 1470 (s), 1446 (s), 1356 (w), 1325 (s), 1203 (m), 1158 (s), 1032 (w), 908 (m), 852 (w), 820 (w), 756 (s), 455 (w). ^{1}H NMR (300 MHz, $(CD_3)_2SO$): δ 7.99 (s, 4H, C*H*=N); 7.26 (t, 4H, J_1 = 6.93 Hz, J_2 = 7.01 Hz, Ar); 7.15 (d, 4H, *J* = 7.90 Hz, Ar); 6.90 (d, 4H, *J* = 8.47 Hz, Ar); 6.48 (t, 4H, J_1 = 7.38 Hz, J_2 = 7.14 Hz, Ar); 3.89 (s, 8H, CH_2).

$[Ni_2(L)\subset NaClO_4]\cdot CH_3CN$ (10) and $[Cu_2(L)\subset NaClO_4]$ (11). The two inclusion compounds were obtained in the same way as described below for **10**. To a suspension of $[Ni_2L]$ (0.132 g, 0.20 mmol) in acetonitrile (50 mL) was added 0.28 g (2.0 mmol) of $NaClO_4\cdot H_2O$. The mixture was heated under reflux for 1 h, during which time a clear dark brown solution was obtained. On slow evaporation of the solution at room temperature, diffraction quality crystals of **10** were obtained.

Compound **10**. Yield: 0.12 g (70%). Anal. Calcd for $C_{35}H_{31}N_5O_8Ni_2NaCl$: C, 50.87; H, 3.75; N, 8.48. Found: C, 50.81; H, 3.69; N, 8.42. FT-IR (KBr, *υ*/cm^{-1}): 3444 (w, br), 2922 (w), 1618 (s), 1539 (s), 1471 (m), 1452 (s), 1358 (w), 1319 (m), 1209 (w), 1120 (s), 1084 (s), 908 (w), 752 (m), 739 (m), 683 (w), 652 (w), 621 (m), 590 (w), 553 (w), 463 (m).

Compound **11**. Anal. Calcd for $C_{33}H_{28}N_4O_8Cu_2NaCl$: C, 49.90; H, 3.52; N, 7.05. Found: C, 49.92; H, 3.60; N, 7.17. FT-IR (KBr, *υ*/cm^{-1}): 3443 (w, br), 3047 (w), 2902 (w), 1624 (s), 1537 (s), 1470 (s), 1448 (s), 1317 (m), 1199 (m), 1151 (m), 1122 (m), 1080 (m), 974 (w), 906 (w), 754 (m), 738 (m), 625 (w), 601 (w), 461 (w). μ_{eff} (298 K) = 2.96 μ_B.

X-Ray Structure Determinations. Single crystals of compounds **1**, **3**, **4**, **6**, **7**, and **10** were mounted on glass fibers and coated with perfluoropolyether oil. Intensity data were collected at 123(2) K on a Bruker-AXS SMART APEX II diffractometer equipped with a CCD detector using graphite-monochromated Mo Kα radiation (λ = 0.71073 Å). The data were processed with SAINT,[25] and absorption corrections were made with SADABS.[25] The structures were solved by direct and Fourier methods and refined by full-matrix least-squares based on F^2 using WINGX software of SHELXTL[26] and SHELX-97.[27] The non-hydrogen atoms were refined anisotropically, while the hydrogen atoms were placed at geometrically calculated positions with fixed isotropic thermal parameters. Wherever the positions of the hydrogen atoms could be detected unequivocally, they were referred to as "seen" in the text. The solvents of crystallization in $[Mg_3(HL)_2]\cdot nH_2O$ (**1**) and $[Ni_3L'_2]\cdot 0.5C_7H_8$ (**4**) were found to be highly disordered and could not be refined satisfactorily, and hence they were removed by applying the SQUEEZE option of PLATON.[28] In the case of compound **1**, structures were determined for three different crystals obtained by diffusing hexane to dichloromethane solutions of **1**. However, in none of the cases did the 2θ values for data collection go above 42.5°. We therefore had to accept this limitation. Nevertheless, in all three cases, the unit cell dimensions and the metrical parameters obtained were in excellent agreement with each other. The structural parameters reported here are based on the *R* indices ($I > 2\sigma(I)$), R1 = 0.0442 and wR2 = 0.1187.

Results and Discussion

Synthesis and Characterization of the Complexes. Because of the tetrahedral disposition of the four bidentate salicylaldimine chelating units of 1,1,1,1-tetrakis[(salicylaldimino)methyl]methane (H_4L), two major interaction processes of it with divalent metal ions can be anticipated. (i) Three chelating units of the ligand will first

---

[25] *SAINT*, version 6.02; *SADABS*, version 2.03; Bruker AXS, Inc.: Madison, WI, 2002.

[26] *SHELXTL*, version 6.10; Bruker AXS, Inc.: Madison, WI, 2002.

[27] Sheldrick, G. M. *SHELXL-97*; University of Göttingen: Göttingen, Germany.

[28] PLATON: Spek, A. L. *Acta Crystallogr., Sect. A*, **1990**, *46*, C34.

Scheme 1

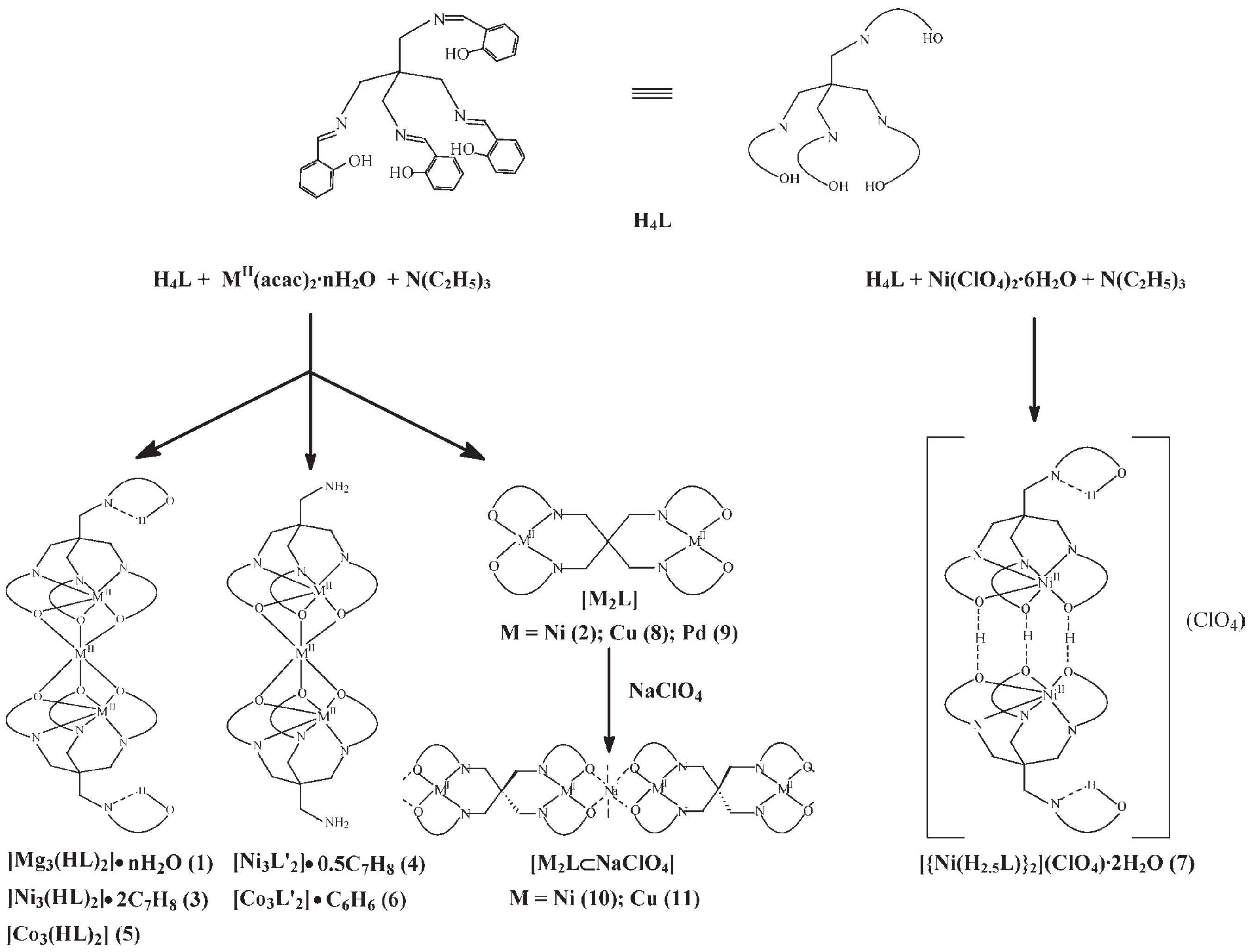

get involved to form a 6-coordinate anionic species $[M(HL)]^-$, and two such species together will then interact with a third metal ion by inducing all six phenolate oxygens to act as bridges to produce a neutral trinuclear complex $[M_3(HL)_2]$. The uncoordinated salicylaldimines of this complex may further interact with a metallic substrate, provided that is sterically allowed. (ii) Metal ions that can adopt a square-based geometry can give rise to neutral dinuclear complexes $[M_2L]$ by deploying two chelating units of the ligand for each of the metal ions. When a metal ion is capable of stabilizing both 4- and 6-coordinate species, a mixture of the two products is likely to be obtained.

Preliminary studies have indicated that for the synthesis of divalent metal complexes of H_4L, metal acetylacetonates $M(acac)_2 \cdot nH_2O$ act as better precursors than simple metal salts. Scheme 1 illustrates the synthesis of $[Mg_3(HL)_2] \cdot nH_2O$ (**1**), $[Ni_2L]$ (**2**), $[Ni_3(HL)_2] \cdot 2C_7H_8$ (**3**), $[Ni3L'_2] \cdot 0.5C_7H_8$ (**4**), $[Co_3(HL)_2]$ (**5**), $[Co_3L'_2] \cdot C_6H_6$ (**6**), $[Cu_2L] \cdot CH_3CN$ (**8**), and $[Pd_2L]$ (**9**) by reacting $M(acac)_2 \cdot nH_2O$ with H_4L and $N(C_2H_5)_3$ in appropriate proportions. For instance, compound **1** has been obtained in near quantitative yield by heating a mixture of Mg, Hacac, H_4L, and $N(C_2H_5)_3$ in methanol–acetonitrile in the ratio 3:6:2:6. When $Ni(acac)_2$ (3 equiv) is reacted with a mixture of H_4L (2 equiv) and $N(C_2H_5)_3$ (6 equiv) in acetonitrile, $[Ni_2L]$ (**2**) precipitates from the boiling solution as the major product, while evaporation of the filtrate followed by recrystallization of the residue from benzene–toluene leads to the isolation of $[Ni_3(HL)_2] \cdot 2C_7H_8$ (**3**) and $[Ni_3L'_2] \cdot 0.5C_7H_8$ (**4**). As expected, quantitative formation of **2** takes place when the ratio of the reactants is 2:1:4. In contrast, the same reaction with $Co(acac)_2 \cdot 2H_2O$ fails to produce $[Co_2L]$. Instead, $[Co_3(HL)_2]$ (**5**) separates out from the boiling solution as the major product, and $[Co_3L'_2] \cdot C_6H_6$ (**6**) is isolated from the filtrate. Subsequent studies, including X-ray structure determinations of **4** and **6**, have revealed that $[Ni_3L'_2]$ and $[Co_3L'_2]$ are the hydrolyzed derivatives of $[Ni_3(HL)_2]$ and $[Co_3(HL)_2]$ whose uncoordinated salicylaldimine is converted to amine (H_3L' is shown in Chart 1). Similar to **2**, $[Cu_2L] \cdot CH_3CN$ (**8**) and $[Pd_2L]$ (**9**) have been obtained by reacting $M(acac)_2 \cdot nH_2O$ with H_4L and $N(C_2H_5)_3$ in the ratio 2:1:4.

An interesting dimeric nickel(II) complex $[\{Ni(H_{2.5}L)\}_2](ClO_4) \cdot 2H_2O$ (**7**) is formed when 2 equivalents each of $Ni(ClO_4)_2 \cdot 6H_2O$ and H_4L are reacted together in the presence of 3 equivalents of $N(C_2H_5)_3$ in acetonitrile (Scheme 1). The X-ray structure of **7** has revealed that in this compound the two monomers are held together by three O···H···O bridges where all the six metal-linked phenols are 50% deprotonated.

Table 1. Crystallographic Data of $[Mg_3(HL)_2]\cdot nH_2O$ (**1**), $[Ni_3(HL)_2]\cdot 2C_7H_8$ (**3**), $[Ni_3L'_2]\cdot 0.5C_7H_8$ (**4**), $[Co_3L'_2]\cdot C_6H_6$ (**6**), $[\{Ni(H_{2.5}L)\}_2](ClO_4)\cdot 2H_2O$ (**7**), and $[Ni_2L\subset NaClO_4]\cdot CH_3CN$ (**10**)

	1	**3**	**4**	**6**	**7**	**10**
empirical formula	$C_{66}H_{58}N_8O_8Mg_3$	$C_{80}H_{74}N_8O_8Ni_3$	$C_{55.50}H_{54}N_8O_6Ni_3$	$C_{58}H_{54}N_8O_6Co_3$	$C_{66}H_{65}N_8O_{14}Ni_2Cl$	$C_{35}H_{31}N_5O_8Ni_2Na$ Cl
fw	1164.13	1451.60	1105.20	1135.88	1347.13	825.51
T, K	120(2)	120(2)	120(2)	120(2)	120(2)	150(2)
cryst syst, space group	monoclinic, $P2(1)/n$	triclinic, $P\overline{1}$	monoclinic, $C2/c$	monoclinic, $P2(1)/n$	monoclinic, $P2(1)/c$	triclinic, $P\overline{1}$
a,Å	15.7341(2)	10.3061(13)	18.889(2)	13.426(3)	17.7694(11)	9.5789(4)
b, Å	24.169(3)	12.5119(15)	12.7412(13)	10.164(2)	20.7840(13)	13.5173(5)
c, Å	18.780(2)	14.0935(18)	20.902(2)	19.825(3)	18.9651(12)	14.4943(6)
α, deg	90	66.988(3)	90	90	90	108.983(2)
β, deg	113.588(3)	80.917(3)	95.858(2)	102.934(6)	117.33(1)	96.689(2)
γ, deg	90	86.728(3)	90	90	90	101.066(2)
V, Å^3	6544.9(14)	1651.7(4)	5004.3(9)	2636.6(10)	6222.3(7)	1709.00(12)
Z, ρ_{calcd}, Mg/m^3	4, 1.181	1, 1.459	4, 1.467	2, 1.431	4, 1.438	2, 1.604
μ, mm^{-1}	0.104	0.914	1.178	0.992	0.722	1.254
$F(000)$	2440	758	2300	1174	2808	848
h, k, l limiting indices	$-15 \le h \le 15$ $-24 \le k \le 24$ $-19 \le l \le 15$	$-13 \le h \le 13$ $-16 \le k \le 14$ $-18 \le l \le 18$	$-20 \le h \le 20$ $-14 \le k \le 13$ $-23 \le l \le 23$	$-16 \le h \le 16$ $-12 \le k \le 12$ $-23 \le l \le 23$	$-23 \le h \le 23$ $-27 \le k \le 25$ $-24 \le l \le 25$	$-11 \le h \le 11$ $-16 \le k \le 16$ $-18 \le l \le 18$
crystal size, mm^3	0.44 × 0.26 × 0.20	0.37x 0.11 × 0.10	0.49 × 0.16 × 0.12	0.38 × 0.26 × 0.19	0.43 × 0.29 × 0.05	0.20 × 0.16 × 0.12
no. of data/restraints/params	7206/0/768	7848/0/450	3599/0/312	4858/0/349	15134/0/823	6927/0/473
no.of reflns [$I > 2\sigma(I)$]	7206	7848	3599	4858	15134	6927
GOF on F^2	0.847	0.857	1.065	0.927	0.932	1.040
final R indices[$I > 2\sigma(I)$]	R1^a = 0.0442 wR2^b = 0.1187	R1^a = 0.0537 wR2^b = 0.0742	R1^a = 0.0337 wR2^b = 0.0867	R1^a = 0.0501 wR2^b = 0.1313	R1^a = 0.0586 wR2^b = 0.1098	R1^a = 0.0634 wR2^b = 0.1733
R indices (all data)	R1^a = 0.0699 wR2^b = 0.1334	R1^a = 0.1064 wR2^b = 0.0870	R1^a = 0.0408 wR2^b = 0.0899	R1^a = 0.0929 wR2^b = 0.1596	R1^a = 0.1354 wR2^b = 0.1277	R1^a = 0.0759 wR2^b = 0.1859

[a] $R1(F) = \sum||F_o| - |F_c||/\sum|F_o|$. [b] $wR2(F^2) = [\sum w(F_o^2 - F_c^2)^2/\sum w(F_o^2)^2]^{1/2}$.

Although the dinuclear $[M_2L]$ complexes of nickel(II), copper(II), and palladium(II) are practically insoluble in acetonitrile, they readily go into solution, except for $[Pd_2L]$, when their suspension in acetonitrile is treated with excess sodium perchlorate (Scheme 1). The inclusion compounds $[M_2L\subset NaClO_4]$ (**10** and **11**) eventually separate out from the solutions on standing.

The compounds under consideration have been characterized by their elemental (C, H, and N) analyses, ESI-MS, IR, UV−vis−NIR, and ^1H NMR spectra, and the relevant results are given in the Experimental Details. The ESI-MSs of $[Ni_3L'_2]\cdot 0.5C_7H_8$ (**4**), $[Co_3L'_2]\cdot C_6H_6$ (**6**), and $[\{Ni(H_{2.5}L)\}_2](ClO_4)\cdot 2H_2O$ (**7**), shown in Figure S1a−c (Supporting Information), indicate that the m/z values for the observed and simulated isotopic distribution patterns of the mono- and dipositive-charged $[M_3L'_2 + H]^+$ and $[M_3L'_2 + 2H]^{2+}$ of **4** and **6** and the monopositive-charged $[\{Ni(H_{2.5}L)\}_2]^+$ of **7** are in excellent agreement, confirming the compositions of the compounds.

The presence of the free amino group in **4** and **6** has been verified by observing a weak band due to υ_{NH} at ca. 3280 cm^{-1} in their IR spectra. Similarly, the observation of the bands due to $\upsilon_{ClO_4^-}$ at ca. 1100 and 625 cm^{-1} confirms the presence of ionic perchlorate in compounds **7**, **10**, and **11**. In all of the complexes, the characteristic band due to $\upsilon_{CH=N}$ is observed between 1620 and 1630 cm^{-1}.

The ^1H NMR spectra of $[Mg_3(HL)_2]\cdot nH_2O$ (**1**) in $CDCl_3$ and $[Pd_2L]$ (**9**) in $(CD_3)_2SO$ (shown in Figure S2a and b, Supporting Information) highlight the essential structural differences that exist between the trinuclear and dinuclear complexes. Thus, in compound **1** (Figure S2a) ,there are 11 signals, including two pairs of singlets due to CH=N (8.46 and 8.12 ppm) and CH_2 (3.74 and 3.61 ppm), and in both cases the proton intensity ratio of the two singlets is 1:3. Further, the 16 aromatic protons of each ligand occur at 7.29, 6.92, 6.90−6.87, 6.54, 6.41, and 6.15 ppm with their intensity ratio being 2:2:2:3:3:3. Additionally, the downfield-shifted singlet observed at 12.79 ppm gets exchanged with D_2O. Taken together, the spectrum suggests that in **1** three pendant salicylaldiminomethyl arms are chelated to a metal center, while the fourth arm remains uncoordinated, whose phenolic OH is intramolecularly hydrogen-bonded to the adjacent imine nitrogen. On the other hand, the spectrum of **9** (Figure S2b) depicts the presence of only one type of CH=N (7.99 ppm), aromatic protons (7.26, 7.15, 6.90, and 6.48 ppm), and CH_2 (3.89 ppm), indicating that all four magnetically equivalent salicylaldiminomethyl units are chelated to the two metal centers in a pairwise fashion. It may be noted that although the spectral features observed for $[Ni_2L]$ (**2**) in $(CD_3)_2NDCO$ are consistent with its diamagnetic behavior in the solid state, in $(CD_3)_2SO$ solution isotropic paramagnetic shifts occur due to the solvent coordination.

Crystal Structures and Stereochemistry. The molecular structures have been determined for four trinuclear compounds, viz. $[Mg_3(HL)_2]\cdot nH_2O$ (**1**), $[Ni_3(HL)_2]\cdot 2C_7H_8$ (**3**), $[Ni3L'_2]\cdot 0.5C_7H_8$ (**4**), and $[Co_3L'_2]\cdot C_6H_6$ (**6**); one dinuclear compound $[\{Ni(H_{2.5}L)\}_2](ClO_4)\cdot 2H_2O$ (**7**); and one inclusion compound $[Ni_2(L)\subset Na](ClO_4)\cdot CH_3CN$ (**10**). The crystallographic data of compounds **1**, **3**, **4**, **6**, **7**, and **10** are given in Table 1.

The ORTEP representations of the trinuclear compounds **1**, **3**, **4**, and **6** are shown in Figure 1a−d. Selected bond distances and angles of **1** are listed in Table 2, while those of **3**, **4**, and **6** are given in Table 3. All four compounds have a common trinuclear core $N_3M(\mu\text{-}O_3)\text{-}M(\mu\text{-}O_3)MN_3$, in which each of the two terminal metal centers are coordinated by three imine nitrogens and three phenolate oxygens provided by three pendant

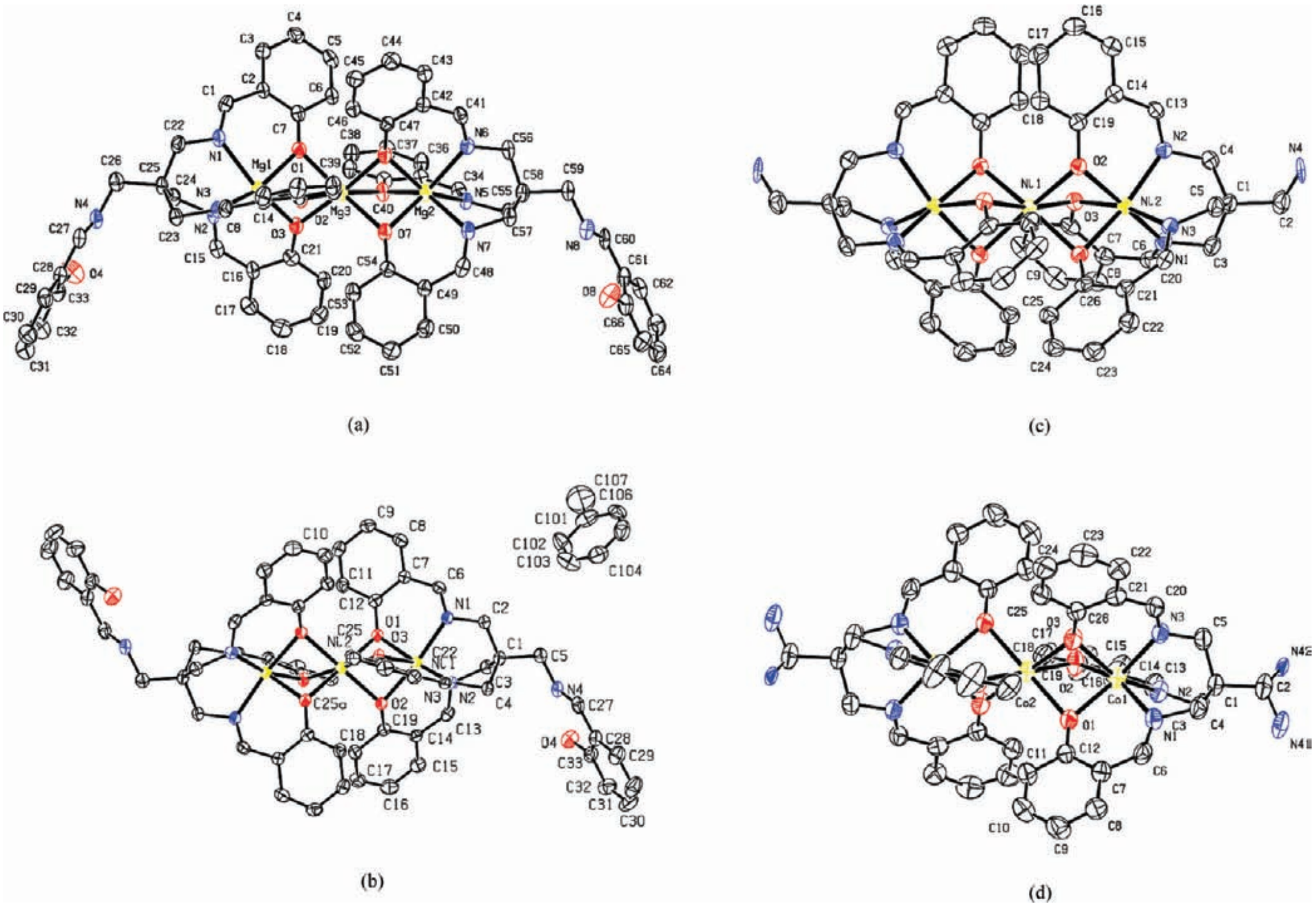

Figure 1. ORTEP representations of $[Mg_3(HL)_2]\cdot nH_2O$ (**1**) (a), $[Ni_3(HL)_2]\cdot 2C_7H_8$ (**3**) (b), $[Ni_3L'_2]\cdot 0.5C_7H_8$ (**4**) (c), and $[Co_3L'_2]\cdot C_6H_6$ (**6**) (d) at 50% probability displacement ellipsoids. Hydrogen atoms are removed for clarity. Disordered water molecules of **1** and toluene of **4** have been removed.

Table 2. Selected Bond Distances and Bond Angles of $[Mg_3(HL)_2]\cdot nH_2O$ (**1**)

bond distances (Å)				bond angle (deg)	
Mg(1)−O(1)	2.056(2)	Mg(2)−N(6)	2.160(3)	O(1)−Mg(1)−N(2)	149.94(10)
Mg(1)−O(2)	2.032(2)	Mg(2)−N(7)	2.177(3)	O(2)−Mg(1)−N(3)	148.43(10)
Mg(1)−O(3)	2.050(2)	Mg(3)−O(1)	2.097(2)	O(3)−Mg(1)−N(1)	149.58(10)
Mg(1)−N(1)	2.183(3)	Mg(3)−O(2)	2.101(2)	O(5)−Mg(2)−N(7)	143.17(10)
Mg(1)−N(2)	2.179(3)	Mg(3)−O(3)	2.080(2)	O(6)−Mg(2)−N(5)	144.27(10)
Mg(1)−N(3)	2.160(3)	Mg(3)−O(5)	2.102(2)	O(7)−Mg(2)−N(6)	145.39(10)
Mg(2)−O(5)	2.069(2)	Mg(3)−O(6)	2.060(2)	O(1)−Mg(3)−O(7)	175.37(9)
Mg(2)−O(6)	2.061(2)	Mg(3)−O(7)	2.073(2)	O(2)−Mg(3)−O(5)	175.07(9)
Mg(2)−O(7)	2.057(2)	Mg(1)···Mg(3)	2.842(1)	O(3)−Mg(3)−O(6)	174.07(9)
Mg(2)−N(5)	2.184(3)	Mg(2)···Mg(3)	2.842(1)	Mg(1)−Mg(3)−Mg(2)	177.62(5)

salicylaldimines of each of the two ligands, and the central metal obtains a MO_6 coordination sphere by sharing all the metal-coordinated phenolate oxygens that act as bridges. Figure 1a and b show that in compounds **1** and **3** where one of the salicylaldimines remains uncoordinated, the phenolic OH and the imine nitrogen are intramolecularly hydrogen-bonded. On the other hand, the structures of **4** and **6** (Figure 1c and d) reveal that in these compounds the fourth salicylaldimine is replaced by an amino group. Clearly, the azomethine linkage of the uncoordinated salicylaldimine moiety of HL^{3-} is hydrolyzed to produce L'^{3-} (Chart 1).

Inspection of the metrical parameters of the trinuclear compounds (Table 3) reveals that for the six-coordinate terminal metals the trans angles deviate substantially from 180°, indicating considerable distortions from regular octahedral geometry. The coordination polyhedra of **1**, **3**, **4**, and **6** shown in Figure 2a−d provide perspective views of the nature of trigonal distortions that are associated with each of the metal centers. The extent of trigonal distortion is given by the twist angle ϕ (shown in Figure 3), which is 0° for trigonal prism (D_{3h}) and 60° for both trigonal antiprism (D_{3d}) and octahedron (O_h). A wide range of ϕ values have been reported in the literature[29] for metal chelates. In the

---

[29] (a) Stiefel, E. I.; Brown, G. F. *Inorg. Chem.* **1972**, *11*, 435. (b) Kepert, D. L. *Inorg. Chem.* **1972**, *11*, 1561. (c) Larsen, E.; La Mar, G. N.; Wagner, B. E.; Parks, J. E.; Holm, R. H. *Inorg. Chem.* **1972**, *11*, 2652. (d) Dymock, K. R.; Palenik, G. J. *Inorg. Chem.* **1975**, *14*, 1220. (e) Kirchner, R. M.; Meali, C.; Bailey, M.; Howe, N.; Torre, L. P.; Wilson, L. J.; Andrews, L. C.; Rose, N. J.; Lingafetter, E. C. *Coord. Chem. Rev.* **1987**, *77*, 89. (f) Drew, M. G. B.; Harding, C. J.; McKee, V.; Morgan, G. G.; Nelson, J. *J. Chem. Soc., Chem. Commun.* **1995**, 1035. (g) Beswick, C. L.; Schulmoz, J. M.; Stiefel, E. I. *Prog. Inorg. Chem.* **2004**, *52*, 55.

Table 3. Selected Bond Distances and Bond Angles for $[Ni_3(HL)_2]\cdot 2C_7H_8$ (**3**), $[Ni_3L'_2]\cdot 0.5C_7H_8$ (**4**), and $[Co_3L'_2]\cdot C_6H_6$ (**6**)

3				**4**				**6**			
bond distance (Å)		bond angle (deg)		bond distance (Å)		bond angle (deg)		bond distance (Å)		bond angle (deg)	
Ni(1)−O(1)	2.076(2)	O(1)−Ni(1)−N(3)	165.55(9)	Ni(1)−O(1)	2.0681(19)	O(1)#^{b} −Ni(1)−O(2)	170.32(7)	Co(1)−O(1)	2.072(3)	O(1)−Co(1)−N(3)	151.17(13)
Ni(1)−O(2)	2.059(2)	O(2)−Ni(1)−N(1)	166.26(9)	Ni(1)−O(2)	2.0565(19)	N(1)−Ni(2)−O(2)	168.13(9)	Co(1)−O(2)	2.100(3)	O(2)−Co(1)−N(1)	155.62(13)
Ni(1)−O(3)	2.0536(19)	O(3)−Ni(1)−N(2)	165.24(9)	Ni(1)−O(3)	2.0850(19)	N(2)−Ni(2)−O(1)	167.44(9)	Co(1)−O(3)	2.104(3)	O(3)−Co(1)−N(2)	151.06(14)
Ni(1)−N(1)	2.048(2)	O(1)−Ni(2)−O(1)#^{a}	180.0	Ni(2)−O(1)	2.0549(19)	N(3)−Ni(2)−O(3)	166.85(9)	Co(1)−N(1)	2.116(4)	O(1)−Co(2)−O(1)#^{c}	180.0
Ni(1)−N(2)	2.043(3)	Ni(1)−Ni(2)−Ni(1′)	180.0	Ni(2)−O(2)	2.0456(19)	Ni(2)−Ni(1)−Ni(2′)	177.92(8)	Co(1)−N(2)	2.088(4)	Co(1)−Co(2)−Co(1′)	180.0
Ni(1)−N(3)	2.038(3)	Ni(1)−O(1)−Ni(2)	85.20(7)	Ni(2)−O(3)	2.0498(19)	Ni(2)−O(1)−Ni(1)	85.77(7)	Co(1)−N(3)	2.095(4)	Co(1)−O(1)−Co(2)	88.33(8)
Ni(2)−O(1)	2.1078(19)	Ni(1)−O(2)−Ni(2)	86.86(7)	Ni(2)−N(1)	2.035(2)	Ni(2)−O(2)−Ni(1)	86.31(7)	Co(2)−O(1)	2.112(3)	Co(1)−O(2)−Co(2)	88.50(8)
Ni(2)−O(2)	2.060(2)	Ni(1)−O(3)−Ni(2)	87.21(8)	Ni(2)−N(2)	2.033(2)	Ni(2)−O(3)−Ni(1)	85.46(7)	Co(2)−O(2)	2.078(3)	Co(1)−O(3)−Co(2)	87.92(8)
Ni(2)−O(3)	2.052(2)			Ni(2)−N(3)	2.034(2)			Co(2)−O(3)	2.096(3)		
Ni(1)···Ni(2)	2.832(2)			Ni(1)···Ni(2)	2.806(4)			Co(1)···Co(2)	2.9091(5)		

[a] Symmetry transformations used to generate equivalent atoms: #, $-x$, $-y$, $(-z+2)$. [b] Symmetry transformations used to generate equivalent atoms: #, $-x$, y, $(-z+1/2)$. [c] Symmetry transformations used to generate equivalent atoms: #, $-x$, $-y$, $-z$

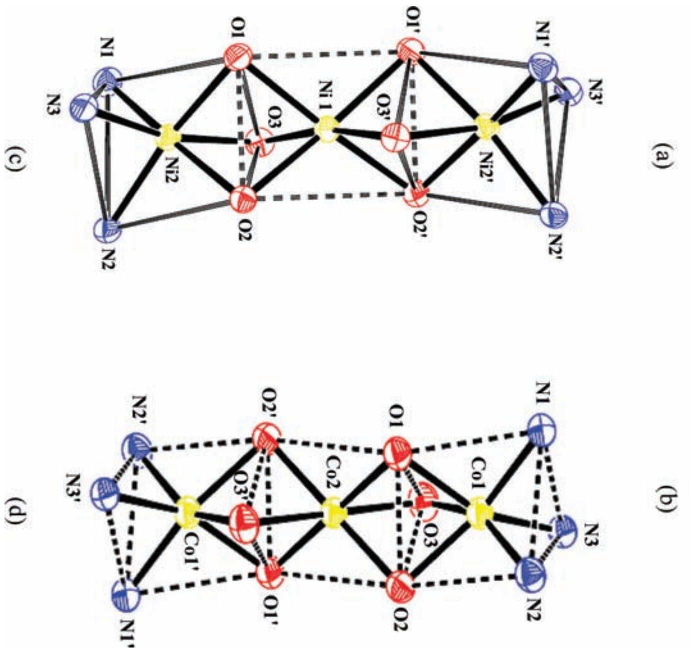

Figure 2. Coordination polyhedra of $[Mg_3(HL)_2]\cdot nH_2O$ (**1**) (a), $[Ni_3(HL)_2]\cdot 2C_7H_8$ (**3**) (b), $[Ni_3L'_2]\cdot 0.5C_7H_8$ (**4**) (c), and $[Co_3L'_2]\cdot C_6H_6$ (**6**) (d).

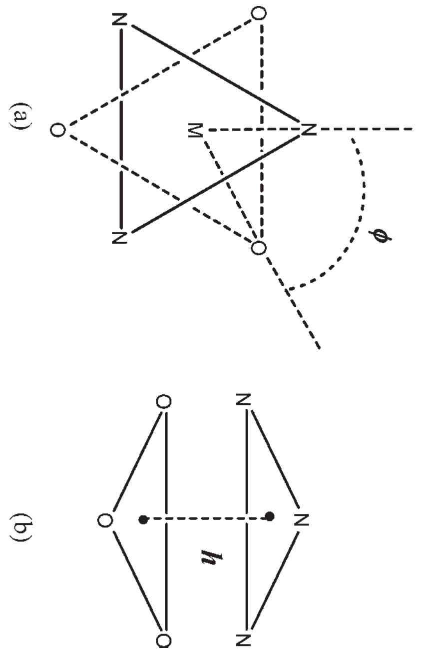

Figure 3. Illustration of twist angle (ϕ) and centroid-to-centroid distance (h) between N_3 and O_3 donor planes.

Table 4. Trigonal Twist Angle (ϕ), Angle between Trigonal Planes (θ), Distance between Trigonal Planes (h), Metal···Metal Distance ($M_t \cdots M_c$), Intermetallic Angle ($M_t-M_c-M_t$), Coordination Geometry of Metal, and Chirality of Trinuclear Compounds **1**, **3**, **4**, and **6**

compd	ϕ (deg)[a]	θ (deg)[b]	h (Å)[c]	$M_t \cdots M_c$ (Å)	$M_t-M_c-M_t$ (deg)	coordination geometry[d,e]	chirality[f]
$[Mg_3(HL)_2]\cdot nH_2O$ (**1**)	20.1 (M_t, Mg1)	0.8	2.778	2.842	177.6	TP (64%)	Λ···Δ
	13.1 (M_t, Mg2)	0	2.805	2.842		TP (73%)	
	66.8 (M_c, Mg3)					OCT[g]	
$[Ni_3(HL)_2]\cdot 2C_7H_8$ (**3**)	42.9 (M_t, Ni1/1′)	0.3	2.651	2.832	180.0	TP (29%)	Δ···Δ
	60.0 (M_c, Ni2)					Oct[h]	
$[Ni_3L'_2]\cdot 0.5\ C_7H_8$ (**4**)	46.3 (M_t, Ni2/2′)	1.0	2.596	2.806	177.9	TAP (77%)	Λ···Δ
	46.7 (M_c, Ni1)					TAP (78%)	
$[Co_3L'_2]\cdot C_6H_6$ (**6**)	26.0 (M_t, Co1/1′)	0.9	2.749	2.909	180.0	TP (57%)	Δ···Δ
	60.0 (M_c, Co2)					OCT[i]	

[a] Average values of ϕ for the terminal metals (M_t) and central metal (M_c). [b] Dihedral angle between the trigonal N_3 and O_3 donor planes. [c] Distance between the centroids of the N_3 and O_3 planes. [d] TP, trigonal prism; TAP, trigonal antiprism; OCT, octahedral. [e] Value in parentheses indicates percentage of distortion from octahedral geometry. [f] Orientations of three N and O^- donors around each of the two terminal metals viewed along the intermetal axis provide configurations of the complex. [g] Axially compressed octahedron. [h] Axially elongated octahedron. [i] Regular octahedron.

context of trigonal distortions, the dihedral angle between the two trigonal planes θ and the separation between the centroids of these two planes h are also taken into consideration to define coordination geometry. The values of ϕ, θ, h, the $M_t \cdots M_c$ (t = terminal, c = central) distance, the $M_t-M_c-M_t$ angle, and the overall geometry of the metal centers in compounds **1**, **3**, **4**, and **6** are summarized in Table 4.

It may be noted in Figure 2a that the terminal metals Mg(1) and Mg(2) in compound **1** are not crystallographically equivalent; their ϕ values are 20.1° and 13.1°, respectively. Accordingly, the distortions from octahedron (OCT) to trigonal prism (TP), that is, OCT → TP, are 64% for Mg(1) and 73% for Mg(2). For the central $Mg(3)O_6$ coordination sphere, the trans O−Mg(3)−O angles (av. 175°) deviate from 180° and $\phi = 66.8°$ also deviates from the ideal value of an octahedron. Further, the axial Mg(3)−O(3)/O(6) distances (av. 2.070 Å) are somewhat shorter relative to those in the equatorial plane (av. 2.094 Å), indicating a slightly tetragonally compressed geometry. Despite the crystallographic nonequivalence of the two terminal metal centers Mg(1) and Mg(2), their distances from the central metal Mg(3) are identical, 2.842 (1)Å, even as the intermetallic angle Mg(1)−Mg(3)−Mg(2) = 177.62° deviates slightly from linearity.

In compound **3** (Figure 2b), the terminal metals Ni(1)/Ni(1′) are equivalent, and the twist angle ϕ (42.9°) indicates that OCT → TP distortion is 29%. For the central nickel Ni(2), trans O−Ni(2)−O angles are all 180°, and the twist angle is also 60°. However, the trans-axial Ni(2)−O(1)/O(1′) distance (2.1078 Å) is appreciably longer relative to the in-plane Ni(2)−O distances (av. 2.056 Å), indicating a tetragonally elongated (D_{4h}) geometry of $Ni(2)O_6$. The distance between the terminal and the central metal is 2.832 Å, while the intermetallic angle is 180°.

Figure 2c shows that in compound **4**, the crystallographically equivalent terminal metals Ni(2)/Ni(2′) as well as the central metal Ni(1) are all distorted toward trigonal antiprism (TAP) geometry. The twist angles 46.3° for Ni(2)/Ni(2′) and 46.7° for Ni(1) are attributed to 77% and 78% TAP distortions. In this case, the distance between the two adjacent metal centers is 2.806 Å, and the angle Ni(2)−Ni(1)−Ni(2′) is 177.9°.

Finally, in compound **6** (Figure 2d), the values of ϕ for the terminal Co(1)/Co(1′) and central Co(2) metals are 26° and 60°, respectively; that is, for Co(1)/Co(1′) OCT → TP distortion is 57%. The central $Co(2)O_6$ coordination sphere is a nearly perfect octahedron because, aside from the trans-axial O−Co(2)−O angles being 180° and ϕ = 60°, all six Co(2)−O bond distances are nearly equal (av. 2.093 Å). The distance between the terminal and central metals is 2.9091 Å, and the angle Co(1)−Co(2)−Co(1′) is 180°.

A second important structural aspect of the trinuclear compounds is their chiralities. Although the ligand itself is achiral, the orientations of the three six-membered N−C−C−C−O−M chelate rings around each terminal metal center induce either a Λ or Δ configuration. The stereochemical configurations of the front and backside metal centers viewed along the intermetal axis are shown in Figure 4 for compounds **1**, **3**, **4**, and **6**. The overall chiralities of the compounds are listed in Table 4. In terms of chirality descriptors,[30] compounds **3** and **6** are both homochiral; that is, they can have either the Δ···Δ or Λ···Λ configuration. However, since both compounds belong to centrosymmetric space groups, therefore, the pairs ΔΔ and ΛΛ coexist in equal amounts, to produce racemic crystals of **3** and **6**. On the other hand, compounds **1** and **4** both being heterochiral Λ···Δ, their crystals are obtained in the *meso* form. Accordingly, none of these compounds exhibit a CD spectrum.

The packing diagrams of the trinuclear compounds have revealed that there are several short contacts between either a methylene hydrogen atom or an aromatic hydrogen atom and the centroid of the π cloud of another aromatic ring. These $C-H\cdots\pi$ interactions are mostly intermolecular in nature. Compounds **3** and **6** each exhibit one intramolecular $C-H\cdots\pi$ interaction in addition to the intermolecular ones. Generally, the upper acceptable limit for the distance of a C−H hydrogen atom from the centroid of an aromatic ring in a $C-H\cdots\pi$ interaction is 3.5 Å.[31] The metrical parameters for $C-H\cdots\pi$ interactions in compounds **1**, **3**, **4**, and **6** (Table 5) indicate that the $H\cdots\pi$ distances range from

---

(30) (a) Saito, Y. *Inorganic Molecular Dissymmetry*; Springer-Verlag: Berlin, 1979. (b) von Zelewsky, A. *Stereochemistry of Coordination Compounds*; John Wiley & Sons: Chichester, U.K., 1995.

(31) (a) Nishino, M.; Hirota, M.; Umezawa, Y. *The CH/π Interaction* (*Evidence, Nature and Consequences*); Wiley-VCH: New York, 1998. (b) Desiraju, G. R.; Steiner, T. *The Weak Hydrogen Bond* (*IUCr Monograph on Crystallography 9*); Oxford Science Publ.: New York, 1999.

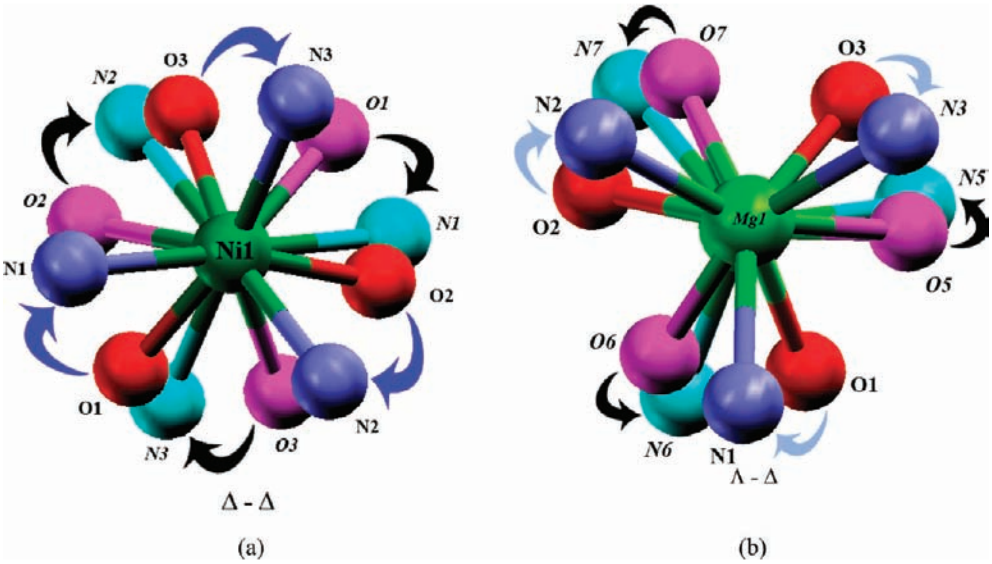

(a) (b)

Figure 4. Heterochiral (Δ···Λ) configuration of compounds **1** and **4** (a) and homochiral (Δ···Δ) configuration of compounds **3** and **6** (b) viewed along their intermetallic axis. The donor atoms of the front side metal are marked as red (oxygen) and blue (nitrogen) spheres, and their direction of orientation is shown by the blue arrow. For the back side metal, the donor atoms (in italics) are pink (oxygen) and magenta (nitrogen) spheres, and the black arrow shows the direction of orientation.

Table 5. Metrical Parameters for C − H···π Interactions in Compounds **1**, **3**, **4**, and **6**

compd	C−H···π[a] atoms	H···π distance (Å)	C−H···π angle (deg)	symmetry code
$[Mg_3(HL)_2]\cdot5H_2O$ (**1**)	C(23)−H(23B)···πC(35)···C(40)[b]	2.727	135.5	1/2 + x, 1/2 −y,1/2 + z; −1/2 + x, 1/2 − y, −1/2 + z
	C(12)−H(12)···πC(61)···C(66)[b]	2.833	142.5	1/2 + x, 1/2 − y, 1/2 + z; −1/2 + x, 1/2 − y, −1/2 + z
	C(38)−H(38)···πC(28)···C(33)[b]	2.836	143.5	1/2 + x, 1/2 − y, 1/2 + z; −1/2 + x, 1/2 − y, −1/2 + z
	C(55)−H(55B)···πC(9)···C(14)[b]	2.697	139.6	1/2 + x, 1/2 − y, 1/2 + z; −1/2 + x, 1/2 − y, −1/2 + z
$[Ni_3(HL)_2]\cdot2C_7H_8$ (**3**)	C(106)−H(10F)···πC(21)···C(26)[b]	2.684	154.2	1 − x, 1 − y, 1 − z
	C(4)−H(4A)···πC(21)···C(26)[b]	2.997	126.9	1 − x, −y, 2 − z
	C(15)−H(15)···πC(101)···C(106)[b]	3.262	165.1	1 − x, −y, 1 − z
	C(18)−H(18)···πC(7)···C(12)[c]	2.917	128.4	−x, −y, 2 − z
$[Ni_3L'_2]\cdot0.5C_7H_8$ (**4**)	C(22)−H(22)···πC(14)···C(19)[b]	2.857	131.1	1/2 − x, 1/2 + y, 1/2 − z; 1/2 − x, −1/2 + y, 1/2 − z
$[Co_3L'_2]\cdot C_6H_6$ (**6**)	C(5)−H(5A)···πC(21)···C(26)[b]	2.524	141.0	x, −1 + y, z
	C(5)−H(5B)···πC(21)···C(26)[b]	3.430	77.2	−x, 1 − y, −z
	C(25)−H(25)···πC(14)···C(19)[c]	3.277	111.1	−x, −y, −z

[a] π designates the centroid of the aromatic ring. [b] Intermolecular C−H···π interaction. [c] Intramolecular C−H···π interaction.

2.5 to 3.4 Å, albeit a majority of them lie between 2.6 and 2.9 Å. As will be seen later, the loss of solvent of crystallization toluene from $[Ni_3(HL)_2]\cdot2C_7H_8$ (**3**) takes place at an appreciably higher temperature. In compound **3**, the connectivities between the solvent of crystallization (toluene) and the core complex ($[Ni_3(HL)_2]$) are established by two C−H···π interactions (Table 5). Moreover, as could be seen in Figure S3 (Supporting Information), along the *c* axis, toluene molecules of **3** are trapped between two layers of $[Ni_3(HL)_2]$. Clearly, solvent trapping and C−H···π interactions have a synergistic effect on augmenting the thermal stability of **3**.

$[\{Ni(H_{2.5}L)\}_2](ClO_4)\cdot2H_2O$ (7). The structure of compound **7** (shown in Figure 5) consists of two similar, but not identical, mononuclear NiN_3O_3complex cores that are formed by the chelation of three salicylaldimine moieties of H_4L with a nickel(II) ion, two uncoordinated water molecules, and a perchlorate anion. Of the two water molecules, the oxygen atom of one is disordered over two sites O(201) and O(202) and their fractional occupancies 0.87 and 0.13, respectively. The two metal cores in **7** are held together strongly by three hydrogen bridges, whose hydrogen atoms H(1) to H(3) were "seen" (inset of Figure 5). Similar to **1** and **3**, the phenolic OH of the uncoordinated salicylaldimine of each ligand remains intramolecularly hydrogen-bonded to the imine nitrogen. Selected bond distances and angles of **7**, including those of the hydrogen bridges, are given in Table 6. It may be noted that all three O···O distances of the hydrogen bridges are similar (2.481(7)Å), while the six O···H distances in the three O···H···O bridges lie between 1.16 and 1.33 Å (av. 1.27 Å). Interestingly, the average O···H distance of **7** is 1.5 times that of the average O−H distance (0.85 Å) observed in phenols. Clearly, all six metal-coordinated phenols in **7** are 50% deprotonated, and as such they may be regarded as *hemiphenolate* bonds. In the two NiN_3O_3 coordination spheres, the N−Ni−O trans angles range from 170° to 173°. The values of trigonal twist angles ϕ for Ni(1) and Ni(2) are respectively 49.1° and 49.7°; that is, OCT → TP distortion is about 17.5% for the metal centers. The average Ni(1)−N and Ni(1)−O distances are 2.030(7) and 2.076(2)Å, respectively, while the corresponding values for Ni(2) are 2.054(7) and 2.072(12)Å. The orientations of the O and N donors along the ligand backbones provide a homochiral Δ···Δ or Λ···Λ configuration, which must be

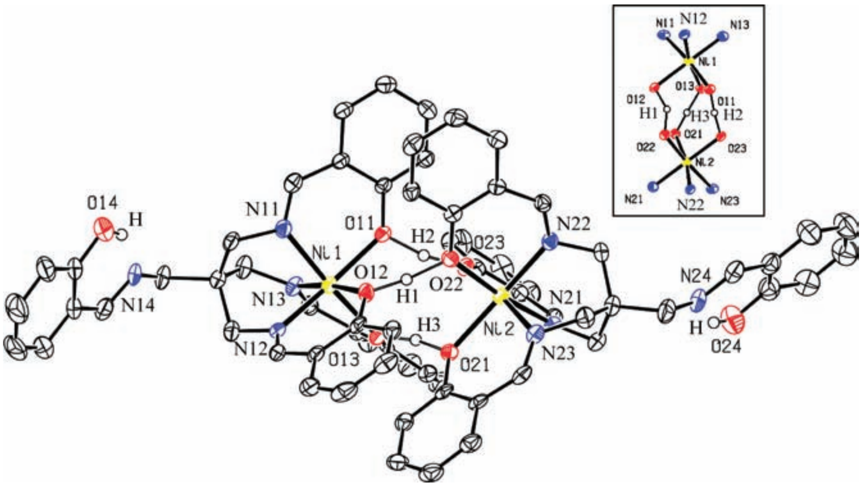

Figure 5. ORTEP representation of the $[\{Ni(H_{2.5}L)\}_2]^+$ ($\mathbf{7}^+$) cation showing 50% probability displacement ellipsoids. Only the phenolic hydrogen atoms H(1), H(2), and H(3) involved in O···H···O hydrogen bondings are shown. The inset illustrates the connectivity between the two $[Ni(N_3O_3)]$ chromophores in the $\mathbf{7}^+$ cation.

Table 6. Selected Bond Distances and Bond Angles and Short Contacts of $[\{Ni_2(H_{2.5}L)\}_2](ClO_4)\cdot 2H_2O$ (**7**)

				hydrogen bonds/short contacts					
bond distance (Å)		bond angles (deg)		distance (Å)				angles (deg)	
Ni(1)−O(11)	2.078(2)	O(11)−Ni(1)−N(12)	171.39(12)	O(14)···N(14)[a]	2.591	H···N(14)	1.845	O(14)···H···N(14)	147.0
Ni(1)−O(12)	2.072(2)	O(12)−Ni(1)−N(13)	173.05(12)	O(24)···N(24)[a]	2.588	H···N(24)	1.848	O(24)···H···N(24)	146.2
Ni(1)−O(13)	2.077(2)	O(13)−Ni(1)−N(11)	170.45(11)						
Ni(1)−N(11)	2.038(4)	O(21)−Ni(2)−N(22)	170.61(11)	O(11)···O(23)[a]	2.481	H(2)···O(11)	1.279	O(11)···H(2)−O(23)	167.8
Ni(1)−N(12)	2.019(3)	O(22)−Ni(2)−N(23)	171.84(11)			H(2)···O(23)	1.216		
Ni(1)−N(13)	2.038(3)	O(23)−Ni(2)−N(21)	172.17(12)	O(12)···O(22)[a]	2.488	H(1)···O(12)	1.220	O(12)···H(1)−O(22)	144.2
Ni(2)−O(21)	2.090(3)					H(1)···O(22)	1.394		
Ni(2)−O(22)	2.064(3)			O(13)···O(21)[a]	2.474	H(3)···O(13)	1.334	O(13)···H(3)−O(21)	166.2
Ni(2)−O(23)	2.061(3)					H(3)···O(21)	1.158		
Ni(2)−N(21)	2.061(3)								
Ni(2)−N(22)	2.048(3)			C(110)···O(1)[b]	3.358	H···O(1)	2.656	C(110)···H···O(1)	128.1
Ni(2)−N(23)	2.054(3)			C(210)···O(2)[b]	3.578	H···O(2)	2.687	C(210)···H···O(2)	149.9
Ni(1)···Ni(2)	4.772			C(211)···O(4)[b]	3.524	H···O(4)	2.596	C(211)···H···O(4)	165.5
				C(219)···O(4)[b]	3.574	H···O(4)	2.711	C(219)···H···O(4)	151.5
				C(102)···O(201)[b]	3.525	H···O(201)	2.718	C(102)···H···O(201)	138.9
				C(103)···O(201)[b]	3.546	H···O(201)	2.673	C(103)···H···O(201)	152.9
				O(1)···O(100)[b]	2.808				
				O(3)···O(202)[b]	2.596				

[a] Intramolecular hydrogen bonds. [b] Intermolecular hydrogen bonds and short contacts. O(1), O(2), O(3), and O(4) represent the oxygen atoms of the perchlorate anion, while O(100), O(201), and O(202) represent the solvated water molecules.

present in equal amounts because of the centrosymmetric space group. The two metal centers in the compound are separated by 4.772 Å. The packing diagram of **7** (Figure S4, Supporting Information) shows that the perchlorate anion and a water molecule are enclosed inside the void space produced by self-assembly.

$[Ni_2L\subset NaClO_4]\cdot CH_3CN$ (10). Perspective views for the three structural representations of the inclusion compound **10** are shown in Figure 6a−c, and selected bond distances and angles of the compound are given in Table 7. Figure 6a shows that in the asymmetric unit, four salicylaldimines of L^{4-} are chelated to two nickel(II) centers in a pairwise fashion, and the phenolate oxygens of both NiN_2O_2 coordination spheres are further coordinated to two sodium ions. Figure 6b shows that each sodium ion obtains a NaO_6 coordination environment by interacting with four symmetry-related phenolate oxygens of two NiN_2O_2 chromophores and two oxygens of two ClO_4^- anions. The space filling diagram of the resulting polymeric network, as shown in Figure 6c, reveals a double-stranded helical structure of **10**.

In the Ni_2L part of **10**, average Ni−O (1.858(2)Å) and Ni−N (1.877(3)Å) distances are nearly equal, all of the trans angles are close to 170°, and the cis angles vary from 82.67° to 94.12°. Thus, the nickel(II) centers have fairly regular square planar geometry. As regards the NaO_6 coordination sphere, the Na−O distances vary from 2.360 to 2.591 Å, of which the four Na−O (phenolate) distances (av. 2.38(2) Å) are shorter while the Na−O (perchlorate) distances (av. 2.56(3) Å) are longer. The O−Na−O trans angles are all exactly 180°. Clearly, the sodium(I) adopts an axially elongated octahedral geometry (D_{4h}).

Absorption Spectra. In DMF, complex $[Ni_2L]$ (**2**) exhibits two bands due to the internal transitions of the ligand, at 315 nm (ε = 11 500 M^{-1} cm^{-1}) and 355 nm (11 300 M^{-1} cm^{-1}), an LMCT band at 425 nm (10 800 M^{-1} cm^{-1}), and a single d−d band at 595 nm (80 M^{-1} cm^{-1}), which are consistent with the spin-paired planar

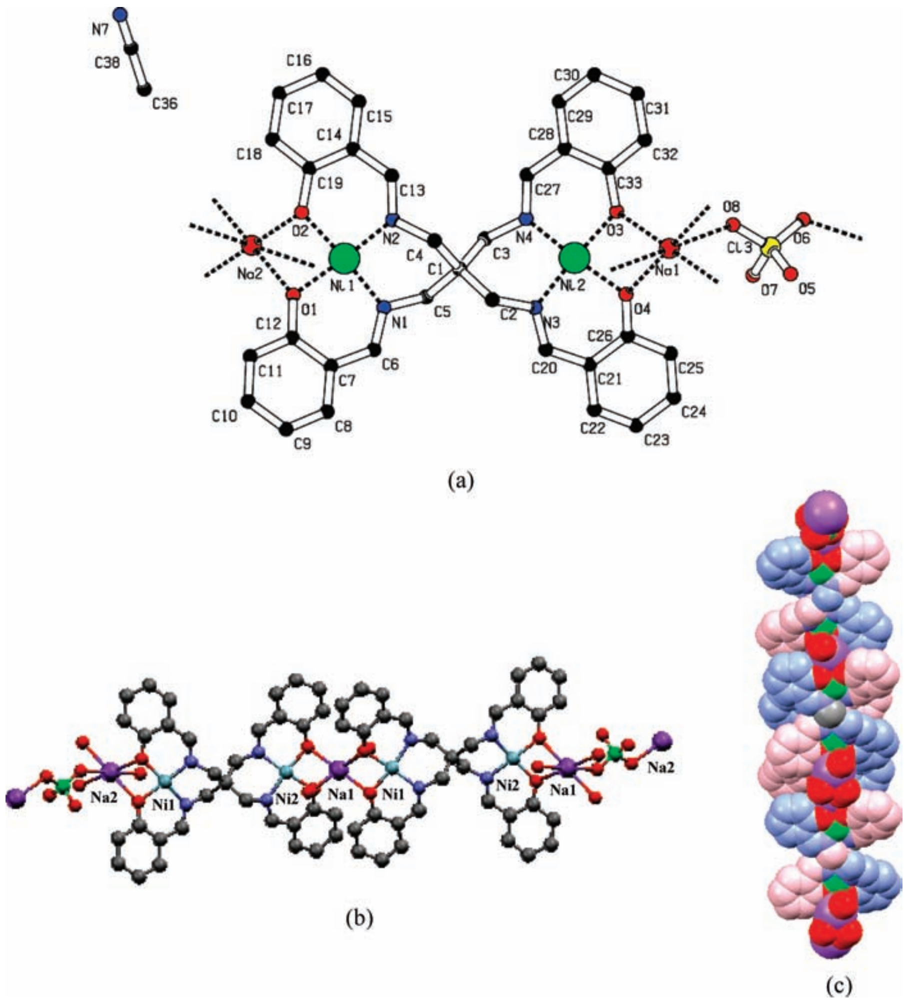

(a)

(b)

(c)

Figure 6. Structural representations of $[Ni_2L{\subset}NaClO_4]\cdot CH_3CN$ (**10**) showing the asymmetric unit (a), coordination environment for Na (b), and space filling helically twisted configuration (c).

Table 7. Selected Bond Distance and Bond Angles of $[Ni_2L{\subset}NaClO_4]\cdot CH_3CN$ (**10**)

				bond distances and angles of Na (1/2) with oxygen atoms (Å)	
bond distance (Å)		bond angle (deg)		bond distance (Å)	
Ni(1)−O(1)	1.857(3)	N(1)−Ni(1)−N(2)	91.85(13)	Na(1)−O(3)	2.376(3)
Ni(1)−O(2)	1.857(3)	N(1)−Ni(1)−O(1)	92.81(14)	Na(1)−O(4)	2.407(3)
Ni(1)−N(1)	1.880(4)	N(2)−Ni(1)−O(2)	94.02(14)	Na(1)−O(8)	2.528(5)
Ni(1)−N(2)	1.869(3)	O(1)−Ni(1)−O(2)	82.67(13)	Na(1)−O(3)#1[a]	2.376(3)
Ni(2)−O(3)	1.856(3)	N(3)−Ni(2)−N(4)	91.67(15)	Na(1)−O(4)#1[a]	2.407(3)
Ni(2)−O(4)	1.863(3)	N(3)−Ni(2)−O(4)	93.00(15)	Na(1)−O(8)#1[a]	2.528(5)
Ni(2)−N(3)	1.879(4)	O(3)−Ni(2)−O(4)	82.79(13)	Na(2)−O(1)	2.400(3)
Ni(2)−N(4)	1.875(3)	N(4)−Ni(2)−O(3)	94.12(14)	Na(2)−O(2)	2.360(3)
Cl(3)−O(5)	1.430(4)	O(1)−Ni(1)−N(2)	170.13(14)	Na(2)−O(1)#3[a]	2.400(3)
Cl(3)−O(6)	1.389(5)	O(2)−Ni(1)−N(1)	169.99(15)	Na(2)−O(2)#3[a]	2.360(3)
Cl(3)−O(7)	1.455(5)	O(3)−Ni(2)−N(3)	169.60(15)	Na(2)−O(6)#4[a]	2.591(5)
Cl(3)−O(8)	1.385(5)	O(4)−Ni(2)−N(4)	169.38(14)	O(3)−Na(1)−O(3)#1	180.00(15)
				O(1)−Na(2)−O(1)#3[a]	180.00(15)

[a] Symmetry transformations used to generate equivalent atoms. #1: $-x + 2, -y + 1, -z$; #3: $-x, -y + 1, -z + 1$; #4: $x - 1, y, z + 1$.

geometry of nickel(II). When the spectrum was recorded in DMSO, the bands due to the $\pi-\pi^*$ transitions of the ligand and the LMCT transitions were shifted to 310 (9600 M^{-1} cm^{-1}), 365 (11 800 M^{-1} cm^{-1}), and 415 nm (9000 M^{-1} cm^{-1}), while the d−d bands are observed at 590 (120 M^{-1} cm^{-1}), 860 (10 M^{-1} cm^{-1}), and 1250 nm (4 M^{-1} cm^{-1}). The positions and intensities of these bands suggest that in DMSO an equilibrium is established between the 4-coordinate planar and a 6-coordinate octahedral species produced by trans-axial interaction of the solvent molecules.

The absorption spectra of the trinuclear nickel(II) complexes **3** and **4** in dichloromethane exhibit similar features. For example, in **3**, the ligand-based $\pi-\pi^*$ transitions occur at 320 (11 200 M^{-1} cm^{-1}) and 370 (22 000 M^{-1} cm^{-1}). The second one seems to be admixed

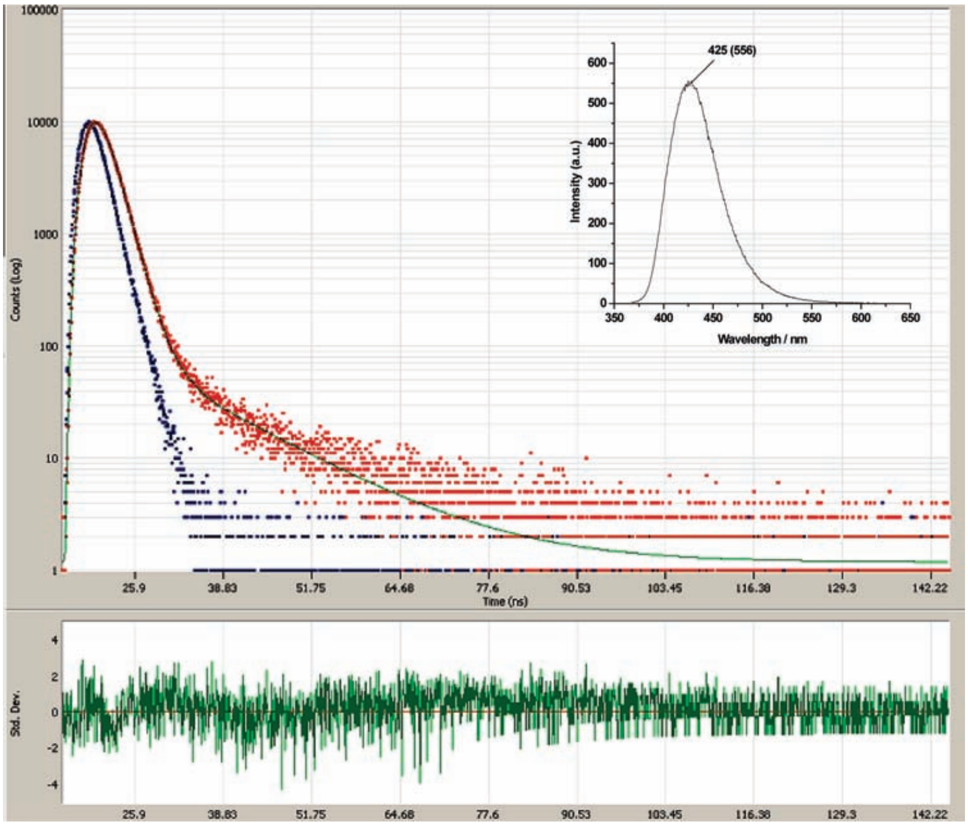

Figure 7. Fluorescent decay of $[Mg_3(HL)_2]\cdot nH_2O$ (**1**) in CH_2Cl_2. The inset shows the luminescence band of **1** excited at 349 nm. The blue, red, and green curves represent the decay profiles of the standard, experimentally observed, and the least-squares fits, respectively.

with the LMCT transition, and the d–d bands are observed at 545 (25 M^{-1} cm^{-1}) and 930 nm (30 M^{-1} cm^{-1}). The corresponding bands in **4** are observed at 325 (9800 M^{-1} cm^{-1}), 380 (18 000 M^{-1} cm^{-1}), 555 (30 M^{-1} cm^{-1}), and 950 (20 M^{-1} cm^{-1}). It may be noted that the d–d bands observed around 540 and 940 nm can be attributed to $^3A_{2g} \rightarrow {}^3T_{1g}(F)$ and $^3T_{2g}$, respectively, in octahedral microsymmetry. In the past, calculations have been carried out for simplified crystal field energy levels of prismatically distorted tris-(bidentate)metal(II) systems,[32] based on which destabilization of TP geometry relative to that of TAP for d^{6-8} configurations has been suggested. Nevertheless, the observed spectral features of weakly trigonally distorted nickel(II) complexes[29c,33] do not show significant differences from regular octahedral nickel(II) complexes. The spectrum recorded for the dimeric nickel(II) complex $[\{Ni(H_{2.5}L)\}_2](ClO_4)\cdot 2H_2O$ (**7**) in DMF shows bands at 320 (24 300 M^{-1} cm^{-1}), 360 (15 600 M^{-1} cm^{-1}), 420 (9000 M^{-1} cm^{-1}), 580 (40 M^{-1} cm^{-1}), and 950 nm (60 M^{-1} cm^{-1}), which again can be assigned in terms of O_h symmetry.

The absorption spectrum of $[Co_3(HL)_2]$ (**5**) in DMF shows a composite band with its peak at 365 nm (26 000 M^{-1} cm^{-1}) and an associated shoulder at about 390 nm. The d–d bands are observed at 580 nm as a shoulder and a broad band spanning from 800 to 1400 nm, whose peak is located at ca. 1020 nm (26 M^{-1} cm^{-1}). The spectral features of this compound are also similar to those of high-spin octahedral cobalt(II) complexes.[34]

Photophysical Study. The photophysical behavior of $[Mg_3(HL)_2]\cdot nH_2O$ (**1**) turns out to be interesting because, despite the fact that ligand H_4L does not exhibit photoluminescence in dichloromethane at room temperature, complex **1** under similar conditions exhibits strong luminescence. The electronic absorption spectrum of **1** in dichloromethane shows two intense bands with their peaks at 262 nm (10 200 M^{-1} cm^{-1}) and 348 nm (53 000 M^{-1} cm^{-1}). These two bands seem to be due to $\pi-\pi^*$ transitions occurring for the aromatic ring and CH=N chromophoric units, respectively, of the metal coordinated ligand. Upon excitation of the band at 348 nm, an intense emission band spanning from 375 to 550 nm with the peak located at 425 nm is observed (see the inset of Figure 7). The excitation spectrum obtained for **1** at different excitation wavelengths shows features that are similar to that of the absorption spectrum with two strong peaks at about 265 and 348 nm, indicating that no structural distortion of **1** occurs in the excited state. The observed Stokes' shift ($\bar{\nu}_{abs} - \bar{\nu}_{em}$) is 5100 cm^{-1} in dichloromethane, which may be compared with the value 6700 cm^{-1} predicted by the Lippert equation.[35] The quantum yield of **1**, measured with respect to perylene in dichloromethane, is 0.075. The photoluminescence behavior of **1** is quite similar to that of the linear trinuclear

---

[32] Gillium, W. O.; Wentworth, R. A. D.; Childers, R. F. *Inorg. Chem.* **1970**, *9*, 1825.

[33] (a) Palmer, R.; Piper, T. S. *Inorg. Chem.* **1966**, *5*, 864. (b) Palmer, R.; Taylor, C. R. *Inorg. Chem.* **1971**, *10*, 2546. (c) Zompa, L. Z.; Margulis, T. N. *Inorg. Chim. Acta* **1980**, *45*, L263.

[34] Lever, A. B. P. *Inorganic Electronic Spectroscopy*, 2nd ed.; Elesevier: Amsterdam, 1984.

[35] Von Lippert, E *Z. Electrochem.* **1957**, *61*, 962.

magnesium(II) complex $\{P(S)[N(CH_3)N{=}CHC_6H_4\text{-}o\text{-}O]_3\}_2$-$Mg_3$ reported by Chandrasekhar et al.,[36] the emission of which was stated to occur from the vertically excited state. The time-resolved luminescence decay of **1** at the ambient temperature (shown in Figure 7) has been analyzed by using the software IBH DAS6 to give a single exponential lifetime $\tau = 18.5 \pm 0.5$ ns, which is typical of fluorescence emission. The calculated natural lifetime of emission ($\tau_n = \tau/\phi$) of 247 ns indicates that in addition to fluorescence from the excited S_1 to S_0 state, other nonradiative processes, especially thermal deactivation, are involved in returning the excited state to the ground state.

Alkali Metal Binding Studies. It has been already noted that acetonitrile insoluble dinuclear complexes $[Ni_2L]$ (**2**) and $[Cu_2L]$ (**8**) readily go into solution upon the addition of excess $NaClO_4$, and from these solutions 1:1 inclusion compounds $[Ni_2L{\subset}NaClO_4]\cdot CH_3CN$ (**10**) and $[Cu_2L{\subset}NaClO_4]$ (**11**) eventually get precipitated. Compound **10** has been shown to have a polymeric structure, in which sodium obtains a 6-fold NaO_6 coordination environment by interacting with four phenolate oxygens and two perchlorate oxygens. Consequently, it has been of interest to assess relative efficacies of complexes $[Ni_2L]$, $[Pd_2L]$, and $[Cu_2L]$ as hosts to accommodate a particular alkali metal ion as a guest and also to find to what extent the affinities of the guest cations Li^+, Na^+, and K^+ differ for a particular host complex. Accordingly, the equilibrium constant K for reaction 1 has been determined at 25 °C in dimethyl sulfoxide.

$$[M_2L] + Alk^+ \overset{K}{\rightleftharpoons} [M_2L{\subset}Alk]^+ \qquad (1)$$

The choice of dimethyl sulfoxide as the solvent was made due to the solubility requirement of the host complexes. The binding constants for $[M_2L]{-}Alk^+$ systems (M^{II} = Ni, Cu, Pd; Alk^+ = Li, Na, K) have been determined by spectrophotometric titrations. Typically, the absorption spectral changes were recorded between 250 and 600 nm for solutions in which the concentration of $[M_2L]$ was kept fixed ($3{-}5 \times 10^{-5}$ M), while the concentrations of alkali metal perchlorates were increased progressively until the limiting spectrum was reached, when no further changes in absorbances occurred. Figure 8a and b show the spectral changes that take place upon the addition of increased amounts of $NaClO_4$ to $[Ni_2L]$ and $LiClO_4$ to $[Cu_2L]$, respectively. As may be noted, in the case of $[Ni_2L]$, augmentation of the intensity of the central peak at 365 nm at the expense of the diminution of intensities of the two terminal peaks at 310 and 415 nm occur. In the terminal spectrum, only the pronouncedly intensified peak at 365 nm is visible. On the other hand, for $[Cu_2L]$, diminution of the intensity of the major peak at 375 nm with a simultaneous increase of absorbance at 330 nm occurs with the progressive addition of $LiClO_4$. In both cases, successive absorption curves pass through well-defined isosbestic points. The overall changes in the spectral profiles of $[Ni_2L]$ and $[Cu_2L]$ are not affected by changing the alkali metal ions, although to reach the limiting spectra, large differences occur in concentrations of the respective alkali metal perchlorates. In contrast to $[Ni_2L]$ and $[Cu_2L]$, no spectral changes occurred for $[Pd_2L]$ with any of the three alkali metal perchlorates, indicating the lack of associative behavior of $[Pd_2L]$.

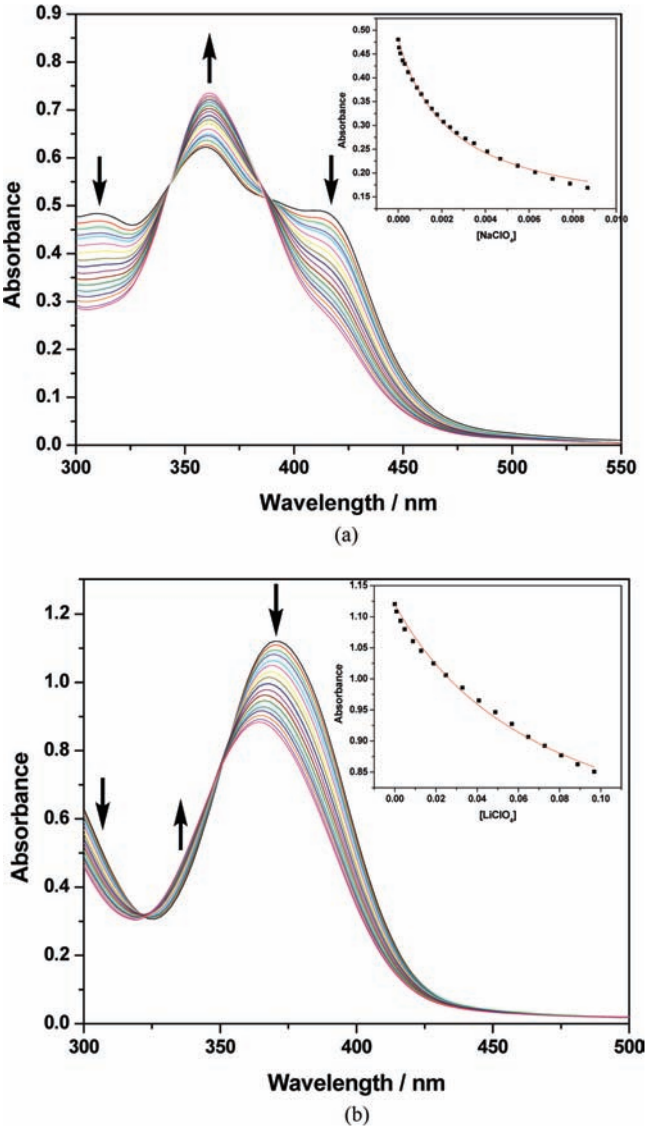

Figure 8. Spectrophotometric titrations of $[Ni_2L]$ with $NaClO_4$ (a) and $[Cu_2L]$ with $LiClO_4$ (b) in $(CH_3)_2SO$. The inset shows the least-squares fit of absorbance versus concentrations of alkali metal perchlorates at a given wavelength.

The binding constants K have been evaluated by a least-squares fit of the absorbance (A) versus alkali metal ion concentration (C_{alk+}) plots (shown as the inset of Figure 8a and b) using eq 2:[37]

$$A = A_0 + \frac{A_{lim} - A_0}{2C_{Alk+}}[C_{Alk+} + C_{M2L} + K^{-1} - \{(C_{Alk+} + C_{M2L} + K^{-1})^2 - 4C_{Alk+}\cdot C_{M2L}\}^{1/2}] \qquad (2)$$

In this equation, A_0, A, and A_{lim} are the absorbances of $[M_2L]$ at a given wavelength without the addition of $(Alk)ClO_4$, with the addition of a particular amount of $(Alk)ClO_4$, and the limiting absorbance reached with a saturation level of added $(Alk)ClO_4$, respectively. C_{M2L} is

---

(36) Chandrasekhar, V.; Azhakar, R.; Bickley, J. F.; Steiner, A. *Chem. Commun.* **2005**, 459.

(37) Bourson, J.; Pouget, J.; Valuer, B. *J. Phys. Chem.* **1993**, *97*, 4552.

Table 8. Binding Constants (*K*) of Alkali Metal Ions in the Host [M_2L] Complexes in Dimethyl Sulfoxide

host	guest	K (mol^{-1} L)[a]
[Ni_2L]	$LiClO_4$	155 ± 3
	$NaClO_4$	417 ± 5
	$KClO_4$	20 ± 2
[Cu_2L]	$LiClO_4$	15 ± 2
	$NaClO_4$	169 ± 2
	$KClO_4$	5 ± 0.2
[Pd_2L]	$LiClO_4$	Nil
	$NaClO_4$	Nil
	$KClO_4$	Nil

[a] Average value of *K* obtained at three different wavelengths.

the total concentration of the [M_2L] complex, and C_{alk+} is the concentration of the added alkali metal perchlorate. The average values of the binding constants evaluated at three different wavelengths are given in Table 8. It may be noted that between the complexes [Ni_2L] and [Cu_2L], the nickel(II) complex shows greater affinity for the alkali metal ions to form inclusion products. Among the three guest alkali metals, the decreased order of their binding constants with both host complexes is $Na^+ > Li^+ > K^+$. The failure of [Pd_2L] even to bind Na^+ might appear surprising. However, consideration of the structure of **10** and the values of the binding constants (Table 8) will bring into focus the importance of the size of the host metal ions to their relative ability to bind a guest cation. Thus, the decreased order of the ionic radii of the host metal ions in a square planar environment,[38] Pd^{2+} (0.64 Å) > Cu^{2+} (0.57 Å) > Ni^{2+} (0.49 Å), appears to be correlated with their binding capacities. Even for the binding of Na^+, the magnitude of difference between the *K* values of [Ni_2L] (417 mol^{-1} L) and [Cu_2L] (169 mol^{-1} L) would suggest an extremely low binding constant for [Pd_2L].

Complementary to spectrophotometric measurements, electrochemical studies carried out for [Cu_2L] in dimethyl sulfoxide with varying quantities of $NaClO_4$ added also provide evidence for Na^+ ion binding. The two copper(II) centers in [Cu_2L] undergo simultaneous one-electron reductions reversibly with $E_{1/2} = -1.03$ V. However, the single peak observed in the square wave voltammogram splits asymmetrically with the incremental addition of $NaClO_4$. This is because the equilibrium mixture of [Cu_2L] and [$Cu_2L\subset Na$]$^+$ undergoes reductions at two different potentials. With a further increase of $NaClO_4$ concentration, the splitted peaks begin to merge together, and finally at the limiting concentration of added $NaClO_4$, a single peak with $E_{1/2} = -0.86$ V is observed again (Figure S5, Supporting Information). Control experiments carried out under the same conditions with tetraethylammonium perchlorate in place of $NaClO_4$ showed that the $E_{1/2}$ value of [Cu_2L] remain unchanged (within the error limit ±10 mV), indicating that the observed changes of potential with the addition of $NaClO_4$ are not due to the variation of supporting electrolyte concentration but due to the relatively easier reduction of cationic [$Cu_2L\subset Na$]$^+$ species.

Proton NMR Spectra of Paramagnetic Compounds. The ^1H NMR spectra of the trinuclear compounds [$Ni_3(HL)_2$]·$2C_7H_8$ (**3**), [$Ni_3L'_2$]·$0.5C_7H_8$ (**4**), and [$Co_3L'_2$]·C_6H_6 (**6**) have been recorded in CD_2Cl_2 at 500 MHz over the range +250 to −50 ppm. As shown in Figure 9, compound **3** exhibits 14 signals, of which five are relatively broad and paramagnetically hyperfine-shifted resonances, while the others are sharp diamagnetic-like resonances occurring between 12 and 2 ppm. The resonances observed at 7.36, 7.24, 7.19, and 2.36 ppm can be attributed to the solvent of crystallization toluene because they are no longer seen in the thermally desolvated product of **3** obtained by heating at 150 °C (see later), while the positions of all other signals remain unchanged. Although the X-ray structure of **3** has revealed the presence of only toluene as the solvent of crystallization, the ^1H NMR spectrum indicates the presence of a small fraction of benzene (7.36 ppm) too, along with the major constituent toluene (7.24, 7.19, and 2.36 ppm). Indeed, the presence of benzene has been confirmed by recording the gas chromatograph of **3** in CH_2Cl_2 (Figure S6, Supporting Information). The two peaks observed with their retention times 2.046 and 3.088 min correspond to benzene and toluene, respectively, and their integrated area ratio of 1:15 is consistent with the lack of observation of benzene in the X-ray structure. The other five sharp signals observed at 11.87, 7.62, 7.05, 6.78, and 3.63 ppm are obviously due to the uncoordinated salicylaldiminomethyl unit whose protons are quite too far away from the metal centers to experience any paramagnetic influence. The relative area ratio of these signals is 1:1:2:2:2, and it may be attributed to the intramolecularly hydrogen-bonded phenolic OH (11.87 ppm), which gets exchanged with D_2O, CH=N (7.62 ppm), four aromatic CH's (7.05 and 6.78 ppm), and CH_2 protons (3.63 ppm).

The chemical shifts and band widths at half-heights (Hz) of the five hyperfine-shifted resonances are 140 (560 Hz), 48.8 (650 Hz), 30.7 (170 Hz), 25.2 (160 Hz), and −0.95 ppm (90 Hz), and all of them have the same integrated areas, which are three times greater relative to the earlier-mentioned O−H···N or CH=N resonances. Assignments of these bands have been made by taking into consideration proximities of the protons of the three equivalent salicylaldiminomethyl units to the coordinated metal center. The Ni···H distances (vide X-ray structure of **3**) according to the atom numbering scheme shown in Chart 2 are methylene H(3A) = 3.32 and H(3B) = 3.83 Å; azomethine H(13A) = 3.82 Å; and aromatic H(18A) = 4.61, H(15A) = 5.29, H(17A) = 6.33, and H(16A) = 6.62 Å. Although seven hyperfine-shifted resonances are expected to be observed for **3**, only five of them could be observed between +250 and −50 ppm. It appears that the signals due to N=CH(13A) and methylene H(3A) lie either beyond the monitored range or are too broad to be seen. In any case, the observed resonances can be assigned in accordance with their Ni···H distances, line widths, and integrated areas as 140 ppm (H3B), 48.8 ppm (H18A), 30.7 ppm (H15A), 25.2 ppm (H17A), and −0.95 ppm (H16A).

The ^1H NMR spectrum of [$Ni_3L'_2$]·$0.5C_7H_8$ (**4**; Figure S7, Supporting Information) also shows five hyperfine-shifted resonances at 141, 48.6, 30.7, 25.3, and −1.05 ppm with similar integrated areas. In the high

---

(38) R Shannon, R. D. *Acta Crystallogr.* **1976**, *A32*, 751.

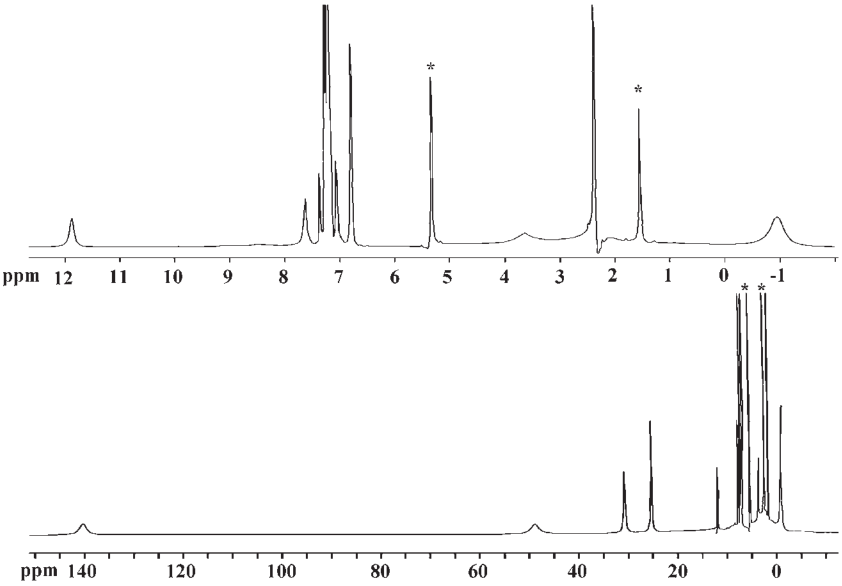

Figure 9. 500 MHz ^{1}H NMR spectrum of $[Ni_3(HL)_2]\cdot 2C_7H_8$ (**3**) in CD_2Cl_2. The high field region in expanded form is shown in the upper part. The solvent peaks are marked with asterisks.

Chart 2

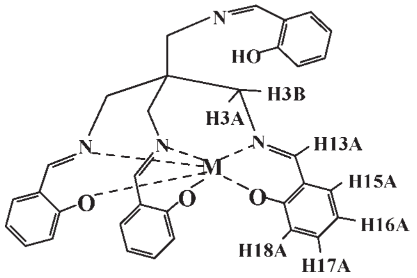

field region, signals only due to toluene and benzene could be observed. Very similar chemical shift values of **3** and **4** are not surprising because the indicated Ni···H distances of **3** are also almost identical for **4**.

The ^{1}H NMR spectrum of $[Co_3L'_2]\cdot C_6H_6$ (**6**) is shown in Figure S8 (Supporting Information). In this case also, five paramagnetic hyperfine-shifted resonances are observed at 231 (810 Hz), 104.6 (160 Hz), −0.35 (65 Hz), −17.4 (80 Hz), and −33.3 ppm (50 Hz). The integrated area ratio of these signals of 2:1:1:1:1 indicates that the resonance observed at 231 ppm is due to the CH_2 protons, while the remaining four are due to the aromatic protons. Again, except for the resonance at 7.38 ppm due to the solvent of crystallization benzene, no other signal could be observed between 2 and 15 ppm.

Magnetic Studies. Variable-temperature (2−300 K) magnetic susceptibility measurements have been carried out for the trinuclear compounds $[Ni_3(HL)_2]\cdot 2C_7H_8$ (**3**), $[Ni_3L'_2]\cdot 0.5C_7H_8$ (**4**), and $[Co_3L'_2]\cdot C_6H_6$ (**6**) and the dimeric compound $[\{Ni(H_{2.5}L)\}_2](ClO_4)\cdot 2H_2O$ (**7**). Two structural aspects of the trinuclear complexes, namely, the linear arrangement of metal centers and equivalence of the terminal metals, define the spin exchange behavior of these compounds. In compound **7**, the hemiphenolate bridges $(O\cdots H\cdots O)^-$ connecting the metal centers, in principle, can act as the pathway for superexchange.

For the nickel(II) complexes **3** and **4**, the spin Hamiltonian is given by eq 3:

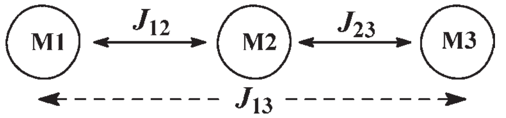

$$\begin{aligned} H = & -2J_{12}S_1\cdot S_2 - 2J_{23}S_2\cdot S_3 - 2J_{13}S_1\cdot S_3 \\ & + D_1\left[S_{z,1}{}^2 - \frac{1}{3}S_1(S_1+1)\right] + D_2\left[S_{z,2}{}^2 - \frac{1}{3}S_2(S_2+1)\right] \\ & + D_3\left[S_{z,3}{}^2 - \frac{1}{3}S_3(S_3+1)\right] + g\beta(S_1\cdot B + S_2\cdot B + S_3\cdot B) \end{aligned} \tag{3}$$

where $S_1 = S_2 = S_3 = 1$, $J_{12} = J_{23}$, $D_1 = D_2$, and all g values are considered to be the same.

The $\chi_M T$ vs T plot for **3** (Figure 10) shows that with the increase of temperature from 4 to 70 K, $\chi_M T$ (and μ_{eff}) values decrease rapidly from 7.32 cm^3 mol^{-1} K (7.70 μ_B) to 4.35 cm^3 mol^{-1} K (5.92 μ_B). However, on further raising the temperature, the lowering of $\chi_M T$ values slows down and ultimately reaches 3.70 cm^3 mol^{-1} K (5.46 μ_B) at 300 K. A nice theoretical fit has been obtained with the parameters $J_{12} = J_{23} = 7.60$ cm^{-1}, $J_{13} = 0$, $D_1 = D_3 = 1.45$ cm^{-1}, $D_2 = 0.41$ cm^{-1}, $g = 2.13$, and TIP $= 300 \times 10^{-6}$ cm^3 mol^{-1} using the program JULX.[39] The magnetic behavior of **4** was found to be very similar to that of **3**. Accordingly, the fitness parameters obtained, $J_{12} = 7.52$ cm^{-1}, $J_{13} = 0$, $D_1 = 1.48$ cm^{-1}, $D_2 = 0.45$ cm^{-1}, $g = 2.15$, and TIP $= 300 \times 10^{-6}$ cm^3 mol^{-1}, were also closely similar. It may be mentioned that, similar to their magnetic properties, the paramagnetically shifted proton

---

(39) Bill, E. *JULX: A Software for Simulation of Molecular Magnetic Data*; Max Planck Institute for Bioinorganic Chemistry: Mülheim, Germany.

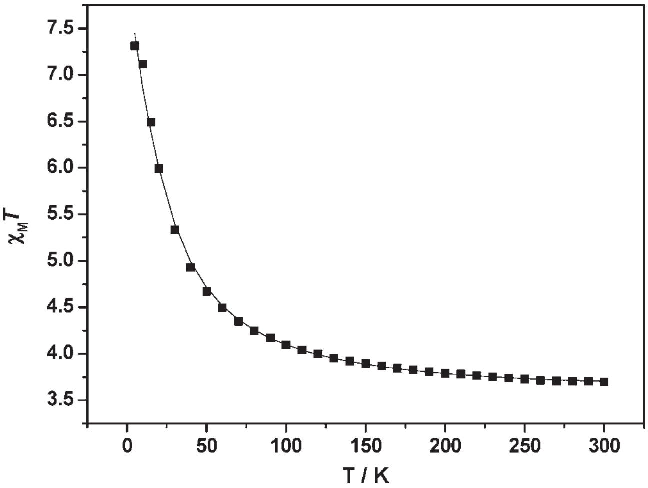

Figure 10. The $\chi_M T$ vs T plot for variable-temperature magnetic susceptibility measurements of $[Ni_3(HL)_2]\cdot 2C_7H_8$ (**3**) in the temperature range 4−300 K. The observed data points are shown as squares (■), and the solid line (—) represents the theoretical least-squares fit.

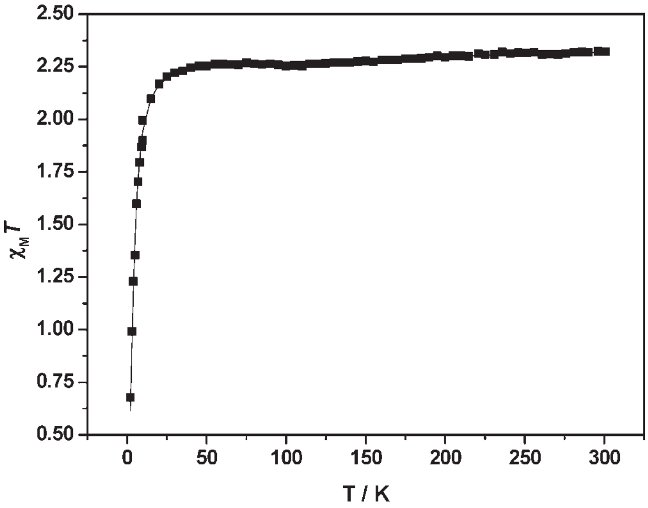

Figure 11. The $\chi_M T$ vs T plot for variable-temperature magnetic susceptibility measurements of $[\{Ni(H_{2.5}L)\}_2](ClO_4)\cdot 2H_2O$ (**7**) in the temperature range 2−300 K. The observed data points are shown as sqaures (■), and the solid line (—) represents the theoretical least-squares fit.

NMR resonances of **3** and **4** are also identical. The ferromagnetic exchange coupling between the adjacent metal centers in **3** and **4** is expected[40,41] because all of the Ni−O−Ni bridge angles in these compounds (av. 86.4° in **3** and 86.0° in **4**) are close to 90°. The absence of any magnetic interaction between the terminal metal centers is not unusual because the intervening distance between the metals in both cases (ca. 5.6 Å) is rather too long for effective through-space spin−spin interaction. It is relevant to compare the exchange coupling constants reported for two related trinickel(II) complexes. Thus, the values reported for $[Ni_3(tsme)_2]$[19a] are $J_{12} = 14.8$ cm^{-1}, $J_{13} = -1.77$ cm^{-1}, and $g = 2.03$. On the other hand, for $[Ni_3\{P(S)(N(CH_3)N{=}CH{-}C_6H_4\text{-}o\text{-}O)_3\}_2]$,[20a] $J_{12} = 3.08$ cm^{-1}, $J_{13} = -0.19$ cm^{-1}, $D = 0.76$ cm^{-1}, and $g = 2.17$. Clearly, the overall magnetic behaviors of these linear trinuclear nickel(II) complexes with similar chromophores are more or less the same with a $S = 3$ spin ground state.

For the dimeric nickel(II) complex **7**, the spin-Hamiltonian is given by eq 4:

$$H = -2JS_1\cdot S_2 + D_1\left[S_{z,1}{}^2 - \frac{1}{3}S_1(S_1+1)\right] + D_2\left[S_{z,2}{}^2 - \frac{1}{3}S_2(S_2+1)\right] + g\beta(S_1\cdot B + S_2\cdot B) \quad (4)$$

where $S_1 = S_2 = 1$ and $D_1 = D_2$.

As shown in Figure 11, the $\chi_M T$ (and μ_{eff}) values remain practically unchanged, 2.32 − 2.23 cm^3 mol^{-1} K (4.33 − 4.24 μ_B), over the temperature range 300 to 35 K. Below 25 K, a sharp drop of $\chi_M T$ occurs, and it reaches a value of 0.66 cm^3 mol^{-1} K (2.31 μ_B) at 2 K. The best fit parameters obtained in this case are $J = -0.23$ cm^{-1}, $D = 9.17$ cm^{-1}, $g = 2.13$, and TIP = 200×10^{-6} cm^3 mol^{-1}. We note that the quality of the theoretical fit vis-à-vis experimental data deteriorated when J was considered to be zero, indicating that the contribution of very weak antiferromagnetic exchange coupling is real. It is worth mentioning that in related $[\{Ni(H_{1.5}tsme)\}_2]^+$, magnetic susceptibility data were simulated[19a] either with $J = -1.00$ cm^{-1} and $g = 2.02$ or with $D = 9.71$ cm^{-1} and $g = 1.93$. At this point, it may be pondered why the D values of **3** and **4** are so different from that of **7**. We believe that the electronic charge difference between phenolate and hemiphenolate bridging oxygens and $O_h \rightarrow D_3$ symmetry lowering to different extents in the two types of compounds profoundly affect their zero-field splittings.

An analysis of temperature-dependent magnetic susceptibility data of exchange-coupled high-spin ($S = 3/2$) dicobalt(II) complexes are problematic because of substantial spin−orbit coupling effects, which get further aggravated with a distortion of cobalt(II) geometry from a pure octahedron.[41] Nevertheless, an isotropic model was developed by Lines[42] for cobalt(II) in pure O_h symmetry by taking into consideration spin−orbit coupling (λ), the orbital reduction factor (κ), and the exchange coupling constant (J). This model was used satisfactorily to analyze magnetic susceptibility data of a few highly symmetric dinuclear cobalt(II) complexes.[43] Subsequently, Sakiyama et al.[44] have further modified this model for axially distorted dicobalt(II) complexes by including the axial splitting parameter (Δ) for the splitting of $^4T_{1g}$ to $^4A_{2g}$ and ^4E_g terms.

As far as the magnetochemistry of linear trinuclear cobalt(II) complexes is concerned, a number of studies have been reported by Cotton and his workers[45] for

---

(40) (a) Nanda, K. K.; Thompson, L. K.; Bridson, J. N.; Nag, K. *J. Chem. Soc. Chem. Commun.* **1994**, 1337. (b) Nanda, K. K.; Das, R.; Thompson, L. K.; Venkatsubramanian, K.; Paul, P.; Nag, K. *Inorg. Chem.* **1994**, *33*, 1188.

(41) Kahn, O. *Molecular Magnetism*; VCH: New York, 1993.

(42) Lines, M. E. *J. Chem. Phys.* **1971**, *55*, 2977.

(43) Munno, G. D.; Julve, M.; Lloret, F.; Faus, J.; Caneschi, A. *J. Chem. Soc., Dalton Trans.* **1994**, 1175.

(44) (a) Sakiyama, H.; Ito, R.; Kumagai, H.; Inoue, K.; Sakamoto, M.; Nishida, Y.; Yamasaki, M. *Eur. J. Inorg. Chem.* **2001**, 2027. (b) Hossain, M. J.; Yamasaki, M.; Mikuriya, M.; Kuribayashi, A.; Sakiyama, H. *Inorg. Chem.* **2002**, *41*, 4058.

(45) (a) Clerac, R.; Cotton, F. A.; Daniels, L. M.; Dunbar, K. R.; Murillo, C. A.; Wang, X. *Inorg. Chem.* **2001**, *40*, 1256. (b) Clerac, R.; Cotton, F. A.; Jeffery, S. P.; Murillo, C. A.; Wang, X. *Inorg. Chem.* **2001**, *40*, 1265. (c) Clerac, R.; Cotton, F. A.; Daniels, L. M.; Dunbar, K. R.; Kirschenbaum, K.; Murillo, C. A.; Finkerton, A. A.; Schultz, A. J.; Wang, X. *J. Am. Chem. Soc.* **2000**, *122*, 6226.

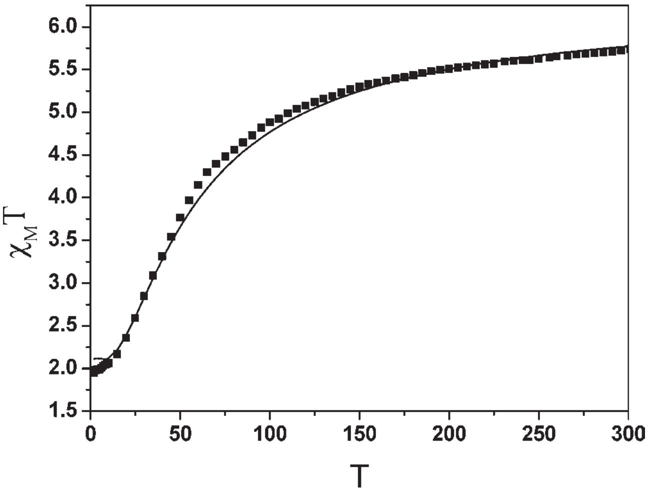

Figure 12. The $\chi_M T$ vs T plot for variable-temperature magnetic susceptibility measurements of $[Co_3L'_2]\cdot C_6H_6$ (**6**) in the temperature range 2−300 K. The observed data points are shown as sqaures (■), and the solid line (—) represents the theoretical least-squares fit.

symmetrical and unsymmetrical $[Co_3(dpa)_4X_2]$ complexes (Hdpa = di(2-pyridyl)amine; X = halogens and pseudohalogens). In the metal−metal bonded symmetrical compounds, over 2−350 K, a gradual spin crossover from a doublet (S = 1/2) to quartet (S = 3/2) state occurs. In a recent study with $[Co_2Pd(dpa)_4Cl_2]$, the cryomagnetic data of the linear array Co^{II}(S = 3/2)Pd^{II}(S = 0)Co^{II}-(S = 3/2) system could be fitted satisfactorily with a model that includes a Hisenberg Hamiltonian and a zero-field splitting operator.[46] The two cobalt(II) centers in this compound are antiferromagnetically coupled.

Very recently, variable-temperature magnetic behavior of a mixed-spin tricobalt(II) complex derived from an oxamidate-*N*,*N*′-bis(3-phenyloxamate) ligand has been reported.[47] In this compound, the terminal metal centers are high-spin, while the central metal is low-spin. For these Co^{II}(S = 3/2)Co^{II}(S = 1/2)Co^{II}(S = 3/2) and Co^{II}(S = 3/2)Co^{III}(S = 0)Co^{II}(S = 3/2) systems, magnetic susceptibility data have been analyzed by taking into consideration λ, κ, Δ, and J parameters. However, we are not aware of any study made with an exchange-coupled Co^{II}(S = 3/2)Co^{II}(S = 3/2)Co^{II}(S = 3/2) linear system where all of the above-mentioned parameters have been considered to fit the cryomagnetic data.

Figure 12 shows the $\chi_M T$ vs T plot for $[Co_3L_2']\cdot C_6H_6$ (**6**). It may be noted that with decreasing temperature the $\chi_M T$ (and μ_{eff}) value decreases gradually from 5.72 cm^3 mol^{-1} K (6.79 μ_B) at 300 K to 4.97 cm^3 mol^{-1} K (6.33 μ_B) at 110 K and then more rapidly to 1.96 cm^3 mol^{-1} K (3.98 μ_B) at 2 K. Clearly, at higher temperatures, all three cobalt(II)'s are in high-spin configuration, and the overall change indicates antiferromagnetic behavior. Treatment of $\chi_M T$ vs T data comprehensively by considering spin−orbit coupling, orbital reduction, and axial splitting along with J_{12}, J_{23}, and J_{13} parameters is beyond the scope of this study. Instead, we have made an approximate analysis of the magnetic data by using the HDVV Hamiltonian given in eq 5

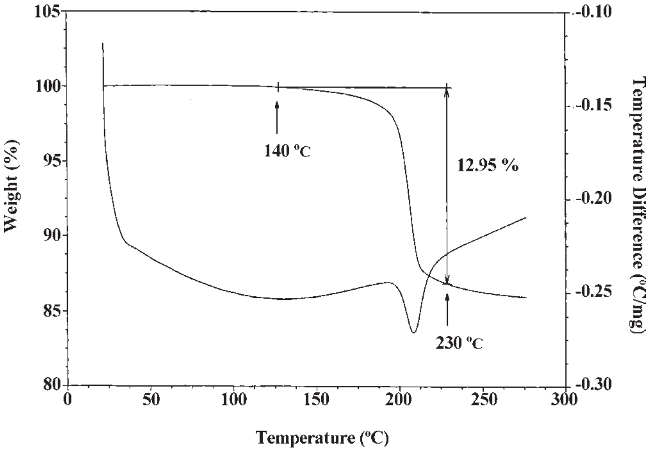

Figure 13. Combined thermogravimetric and differential thermal analysis of $[Ni_3(HL)_2]\cdot 2C_7H_8$ (**3**) in the range 25−300 °C under a nitrogen atmosphere at a heating rate of 5 °C/min.

$$H = -2J_{12}S_1\cdot S_2 - 2J_{23}S_2\cdot S_3 - 2J_{13}S_1\cdot S_3 \qquad (5)$$

As shown in Figure 12, simulation of the experimental data could be made, albeit less satisfactorily, with the fitness parameters J_{12} = J_{23} = −5.73 cm^{-1}, J_{13} = 0, g = 2.13, TIP = 300 × 10−6 cm^3 mol^{-1}, and paramagnetic impurity (PI) = 1%. We note that the magnetic behavior of **6** is similar to that reported for $[Co_3\{P(S)(N(CH_3)N{=}CH{-}C_6H_4\text{-}o\text{-}O)_3\}_2]$ for which J_{12} = J_{23} = −3.13 cm^{-1} and J_{13} = =0.97 cm^{-1}.[20a]

Thermal Studies. The thermal stabilities of $[Ni_3(HL)_2]\cdot 2C_7H_8$ (**3**) and $[Co_3L'_2]\cdot C_6H_6$ (**6**) have been studied over the temperature range 25−300 °C by thermogravimetric (TG), differential thermal analysis (DTA), and differential scanning calorimetric (DSC) measurements. Figure 13 shows the combined TG and DTA of compound **3**, which indicates that the solvated compound remains stable up to 140 °C and desolvation then occurs between 140 and 230 °C. The desolvated product is stable up to 280 °C. Isothermal weight loss measurements carried out at 150 °C have indicated that complete desolvation takes place in 2 h. The observed weight loss (12.95%) is in agreement with the value (12.70%) required for the loss of two toluene molecules. The enthalpy change for desolvation, as obtained from DSC measurement, is 29.9 J g^{-1}, that is, 43.4 kJ mol^{-1}.

In order to find out whether the desolvated product $[Ni_3(HL)_2]$ can absorb toluene vapor to regain the original composition $[Ni_3(HL)_2]\cdot 2C_7H_8$, the isothermally desolvated product was kept at room temperature in a closed container saturated with toluene vapor for 3 days, after which the product was exposed to the atmosphere for 2 h. The TGA of this product showed that from 60 °C onward weight loss began to take place and continued until 180 °C, above which no further change in weight occurred. The observed weight loss of 9.2% corresponds to a composition approaching $[Ni_3(HL)_2]\cdot 1.5C_7H_8$. The powder diffraction patterns of desolvated $[Ni_3(HL)_2]$ as well as $[Ni_3(HL)_2]\cdot 1.5C_7H_8$ were found to be structureless and amorphous. A similar adsorption study carried out with benzene led to the isolation of a product,

---

[46] Rohmer, M.-M.; Lu, I. P.-C.; Lin, J.-C.; Chiu, M.-J.; Lee, G.-H.; Benard, M.; Lopez, X.; Peng, S.-M. *Angew. Chem., Int. Ed.* **2007**, *46*, 3533.

[47] Dul, M.-C.; Pardo, E.; Lescouezec, R.; Chamoreau, L.-M.; Villian, F.; Journaux, Y.; Ruiz-Garcia, R.; Cano, J.; Julve, M.; Lloret, F.; Pasan, J.; Ruiz-Perez, C. *J. Am. Chem. Soc.* **2009**, *131*, 14614.

$[Ni_3(HL)_2]\cdot 1.8C_6H_6$, whose TGA showed 8.0% weight loss. Clearly, desolvation of **3** causes destruction of the crystalline phase and its subsequent exposure to toluene/benzene, while leading to their adsorption but not a revival of a crystalline phase. The adsorption study indicates that there is no preferential choice of toluene over benzene to be caged in the lattice. The apparent composition $[Ni_3(HL)_2]\cdot(C_7H_8)_{1.875}(C_6H_6)_{0.125}$ of **3** seems to have been attained as a consequence of the solubility requirement. In the case of $[Co_3L'_2]\cdot C_6H_6$ (**6**), the loss of benzene begins to take place at 100 °C and continues up to 180 °C. The observed weight loss 6.73% is in agreement with the value 6.84% expected for the evolution of one benzene molecule.

Conclusions and Summary

The wide ranging variation of structure, stereochemistry, and physicochemical properties of complexes of magnesium(II), nickel(II), cobalt(II), copper(II), and palladium(II) that can be brought about by manipulating the coordination behavior of the tetrapodal ligand 1,1,1,1-tetrakis[(salicylaldimino)methyl]methane (H_4L) have been addressed. Five types of compounds, viz. (i) $[Mg_3(HL)_2]\cdot nH_2O$ (**1**), $[Ni_3(HL)_2]\cdot 2C_7H_8$ (**3**), and $[Co_3(HL)_2]$ (**5**); (ii) $[Ni_3L'_2]\cdot 0.5C_7H_8$ (**4**) and $[Co_3L'_2]\cdot C_6H_6$ (**6**); (iii) $[Ni_2L]$ (**2**), $[Cu_2L]$ (**8**), and $[Pd_2L]$ (**9**); (iv) $[\{Ni(H_{2.5}L)\}_2](ClO_4)\cdot 2H_2O$ (**7**); and (v) $[Ni_2L\subset NaClO_4]\cdot CH_3CN$ (**10**) and $[Cu_2L\subset NaClO_4]$ (**11**) were obtained, of which **1**, **3**, **4**, **6**, **7**, and **10** have been structurally characterized. The fourth uncoordinated salicylaldimine moiety of **3** and **5** is hydrolyzed to the amine ending group in **4** and **6**, respectively. The two monomeric complex units in **7** dimerize through three hemiphenolate $(O\cdots H\cdots O)^-$ bridges. All of the trinuclear compounds have a $N_3M^{II}(\mu\text{-}O_{phenolate})_3M^{II}(\mu\text{-}O_{phenolate})_3M^{II}N_3$ core; however, the terminal metal centers in these compounds are distorted to either trigonal prismatic or antiprismatic geometry, albeit the central metal remains predominantly octahedral. Further, the stereochemical configurations of the terminal metal centers are heterochiral $(\Lambda\cdots\cdot\Delta)$ for **1** and **4** but homochiral $(\Delta\cdots\Delta)$ for **3** and **6**. The sodium perchlorate inclusion compound $[Ni_2L\subset NaClO_4]\cdot CH_3CN$ (**10**) has an oligomeric structure, in which the sodium is octahedrally surrounded by six oxygen atoms, four of which are nickel-coordinated phenolate oxygens and two are perchlorate oxygens.

The host–guest bindings between $[M_2L]$ (M = Ni, Cu, Pd) host complexes and alkali metal guest cations (Li^+, Na^+, K^+) have been compared by evaluating their 1:1 binding constants (K). As compared to $[Cu_2L]$, $[Ni_2L]$ acts as a better host, while $[Pd_2L]$ fails to bind any of the guest cations. For the host, the decreasing order of binding constants of the guest cations is $Na^+ > Li^+ > K^+$. On the other hand, the binding abilities of the hosts decrease with the increasing ionic size $Ni^{2+} < Cu^{2+} < Pd^{2+}$.

$[Mg_3(HL)_2]\cdot nH_2O$ (**1**) exhibits strong luminescence (λ_{em} = 425 nm) in dichloromethane at room temperature, although the ligand itself is nonluminescent under the same conditions. The lifetime of fluorescent decay is 18.5 ns, and the quantum yield is 0.075.

$[Ni_3(HL)_2]\cdot 2C_7H_8$ (**3**) and $[Co_3L'_2]\cdot C_6H_6$ (**6**) show considerable thermal stability for the loss of solvent of crystallization. The observed behavior can be related to caging of the solvent molecules in the crystal lattices and the presence of $C-H\cdots\pi$ interactions.

Variable temperature (2–300 K) magnetic susceptibility measurements have indicated the $S = 3$ spin ground state for $[Ni_3(HL)_2]\cdot 2C_7H_8$ (**3**) and $[Ni_3L'_2]\cdot 0.5C_7H_8$ (**4**); the adjacent metal centers in both cases are ferromagnetically coupled with almost the same J values (ca. 7.6 cm^{-1}), while no exchange coupling occurs between the terminal centers. In contrast, the adjacent metal centers in $[Co_3L'_2]\cdot C_6H_6$ (**6**) are involved in antiferromagnetic coupling ($J = -5.7\ cm^{-1}$) and again with no interaction between the terminal centers. The magnetic behavior of $[\{Ni(H_{2.5}L)\}_2](ClO_4)\cdot 2H_2O$ (**7**) is consistent with very weak antiferromagnetic spin-exchange between the $O\cdots H\cdots O$ bridged metal centers ($J = -0.2\ cm^{-1}$), having a major contribution of the zero-field splitting parameter ($D = 9.2\ cm^{-1}$).

Acknowledgment. K.N. is thankful to the Indian National Science Academy for supporting him as an INSA Senior Scientist. Thanks are due to the Department of Science and Technology, Government of India for establishing the National X-ray Diffractometer facility at the Department of Inorganic Chemistry, Indian Association for the Cultivation of Science. Thanks are also due to Mr. Subrata Das, IACS, for TCSPC measurements.

Supporting Information Available: X-ray crystallographic file in CIF format for compounds **1** (CCDC 772279), **3** (CCDC 772280), **4** (CCDC 772281), **6** (CCDC 772282), **7** (CCDC 772283), and **10** (CCDC 772284) and Figures S1–S8. This material is available free of charge via the Internet at http://pubs.acs.org.